Spectroscopy of AlAr and AlKr from 31 000 cm^{-1} to the ionization limit

Scott A. Heidecke,[a] Zhenwen Fu,[b] John R. Colt,[c] and Michael D. Morse
Department of Chemistry, University of Utah, Salt Lake City, Utah 84112

(Received 23 September 1991; accepted 13 April 1992)

Spectra of jet-cooled AlAr and AlKr have been collected over the range from 31 000 cm^{-1} to the ionization limit, using the technique of resonant two-photon ionization spectroscopy with mass spectrometric detection. Adiabatic ionization potentials have been accurately measured for both molecules, and have been estimated for $AlAr_2$ and $AlAr_3$. The spin–orbit splittings in the $X\,^2\Pi$ ground state have been determined for both AlAr and AlKr, and ground-state bond strengths have been accurately measured as $D_0[\mathrm{AlAr}, X_1\,^2\Pi_{1/2}(3p)] = 122.4 \pm 4\ cm^{-1}$ and $D_0[^{27}\mathrm{Al}\,^{84}\mathrm{Kr}, X_1\,^2\Pi_{1/2}(3p)] = 194.7 \pm 0.8\ cm^{-1}$. These values have also been combined with the measured ionization potentials to derive $D_0(Al^+\text{–}Ar) = 982.3 \pm 5\ cm^{-1}$ and $D_0(Al^+\text{–}Kr) = 1528.5 \pm 2\ cm^{-1}$.

I. INTRODUCTION

Since the introduction of supersonic expansions as a tool of optical spectroscopy (initially applied to NO_2 by Smalley, Levy, and Wharton[1,2]), the electronic spectra of a large number of van der Waals complexes have been investigated. These range from simple diatomic complexes such as NaAr,[3,4] SiAr,[5] and AgAr,[6] through more complicated species such as Ag_2Ar (Ref. 7) and I_2He,[8,9] on up to large species such as glyoxal–Ar (Ref. 10) and *s*-tetrazine–acetylene.[11] In most cases, however, only one (or a few) electronic states have been investigated, and no attempt has been made to extrapolate to the electronic structure of the ionized complex. In this paper we report an investigation of the Rydberg states of AlAr and AlKr, and provide accurate measurements of the binding energies of these species for the ground state, several excited states, and the cation. The ionization potentials of these species are also accurately measured, and the solvation of an aluminum cation in argon is investigated. Some interesting dynamics are encountered as well, since certain of the excited electronic states predissociate faster than ionization can occur.

The first spectroscopic study of a rare gas complexed with aluminum was reported by Gardner and Lester.[12] Resonant two-photon ionization (R2PI) spectroscopy was combined with mass spectrometric detection to observe the $B\,^2\Sigma^+(4s) \leftarrow X_1\,^2\Pi_{1/2}(3p)$ system of AlAr, with an origin band at 25 113 cm^{-1}. In this notation (which is used throughout this paper) the designation which follows the term symbol in parentheses provides the orbital occupied by the aluminum valence electron in the separated atom limit. Thus the $B\,^2\Sigma^+(4s)$ state of AlAr is the $^2\Sigma^+$ state which correlates to the $\mathrm{Ar}(^1S_0) + \mathrm{Al}(3s^24s^1, ^2S_{1/2})$ separated atom limit. Gardner and Lester[12] observed and analyzed the 0–0 through 6–0 bands of this $B\,^2\Sigma^+(4s) \leftarrow X_1\,^2\Pi_{1/2}(3p)$ system, from which they derived lower limits on the binding energies of $D_0(X_1) = 133\ cm^{-1}$ and $D_0(B) = 373\ cm^{-1}$ for the $X_1\,^2\Pi_{1/2}(3p)$ and $B\,^2\Sigma^+(4s)$ states, respectively.

A subsequent fluorescence excitation and emission study by Callender, Mitchell, and Hackett[13] focused on the same $B\,^2\Sigma^+(4s) \leftarrow X_1\,^2\Pi_{1/3}(3p)$ band system but expanded the study to include AlAr, AlKr, and AlXe. Ground-state binding energies were estimated as $D_0(X_1, \mathrm{AlAr}) = 136 \pm 65\ cm^{-1}$, $D_0(X_1,\mathrm{AlKr}) = 181 \pm 68\ cm^{-1}$, and $D_0(X_1,\mathrm{AlXe}) = 307 \pm 58\ cm^{-1}$.[13] These same authors have also investigated the $B\,^2\Sigma^+(6s) \leftarrow X_1\,^2\Pi_{1/2}(5p)$ band system of the isovalent indium complexes InAr, InKr, and InXe.[14] Following these studies, a high-resolution investigation of the $B\,^2\Sigma^+(4s) \leftarrow X_1\,^2\Pi_{1/2}(3p)$ band system of AlAr by McQuaid, Gole, and Heaven[15] estimated the ground-state binding energy to be $D_0(X_1,\mathrm{AlAr}) = 165^{+40}_{-10}\ cm^{-1}$. In this work the ground- and excited-state bond lengths were determined as well, giving $r_e(X_1,\mathrm{AlAr}) = 3.79 \pm 0.01$ Å and $r_e(B,\mathrm{AlAr}) = 3.05 \pm 0.01$ Å.[15] A similar investigation of the $B\,^2\Sigma^+(4s) \leftarrow X_1\,^2\Pi_{1/2}(3p)$ and $H\,^2\Sigma^+(5s) \leftarrow X_1\,^2\Pi_{1/2}(3p)$ band systems of AlKr is given in the preceding paper by Fu *et al.*, giving bond lengths of $r_e(X_1,\mathrm{AlKr}) = 3.84 \pm 0.01$ Å, $r_e(B,\mathrm{AlKr}) = 3.03 \pm 0.01$ Å, and $r_e(H,\mathrm{AlKr}) = 3.10 \pm 0.01$ Å.[16]

In related work Schriver *et al.* investigated the ionization potentials of $AlAr_n$ and $Al(N_2)_n$ clusters for *n* ranging from 1 to 60.[17] A tunable ultraviolet laser was used to ionize the clusters at an energy only slightly above threshold, resulting in a mass spectrum which demonstrated icosahedral packing of the argon atoms around the aluminum. Although the diatomic AlAr complex was not the major focus of this paper, its ionization potential was determined to be approximately 5.88 eV, and the ionization potentials of $AlAr_2$ and $AlAr_3$ were determined as 5.81 and 5.75 eV, respectively.

The present investigation of AlAr and AlKr began when argon carrier gas was used in a resonant two-photon ionization study of Al_2.[18] In the course of this work, intense

[a] Present address: E. I. DuPont de Nemours & Company, Textile Fibers Department, Fiber Surface Research, Kinston, NC 28502.
[b] Present address: Analytical Research Department, Sect. 57, Rohm and Haas Company Research Laboratories, 727 Norristown Road, Spring House, PA 19477.
[c] Present address: Department of Chemistry, Rice University, Houston, Texas, 77251.

 0021-9606/92/151692-19$06.00

transitions were observed throughout the ultraviolet at mass 67, corresponding to the AlAr complex. The transitions have now been clearly correlated with the $3s^2ns$, $3s^2np$, $3s^2nd$, and $3s^2nf$ excited states of aluminum. Rydberg series have been assigned out to large values of n (particularly for the nd series, which has been assigned out to $n = 9$). Since aluminum has a low ionization potential [IP(Al) = 5.985 77 eV (Ref. 19)], it has been possible to follow the Rydberg series to the ionization limit, allowing accurate measurements of the ionization potential of the AlAr complex. The dissociation energy was also accurately measured by the observation of a convergence limit in the $3s^23d\ ^1$ set of states. Following this initial work on AlAr, analogous measurements were made on AlKr, allowing a comparison of the two complexes.

Experimental details of this work are provided in Sec. II, followed by a presentation of results in Sec. III. These are discussed further in Sec. IV. Section V then concludes the paper with a summary of our most important findings.

II. EXPERIMENT

The spectra of AlAr and AlKr were investigated using a previously described resonant two-photon ionization apparatus.[20] A metal target disk was machined from stock aluminum (6061 alloy), and was used in a rotating disk vaporization assembly similar to that described by O'Brien *et al.*[21] It was placed in the throat of a pulsed supersonic expansion and vaporized using the second-harmonic radiation of a Q-switched Nd:YAG laser (532 nm, 6–8 mJ/pulse, focused to a spot about 0.5 mm in diameter) (YAG denotes yttrium aluminum garnet). The pulsed nozzle was operated using a backing pressure of 40 psi (gauge) of either pure argon (for the AlAr studies) or 5% krypton in argon (for the AlKr studies). The vaporized aluminum atoms were entrained in the carrier gas and traveled through a channel 2 mm in diameter and approximately 2 cm in length prior to expansion into vacuum.

Following expansion into vacuum, the molecular beam was admitted into a reflectron time-of-flight mass spectrometer through a 5 mm skimmer. A Nd:YAG pumped dye laser was then frequency doubled using an angle-tuned doubling crystal of either potassium dihydrogen phosphate (KDP) or β-barium borate (BBO), and both the fundamental and second-harmonic radiation were directed into the ionization region of the time-of-flight mass spectrometer, counterpropagating with respect to the molecular beam. All of the excited states observed in the present experiments are accessed by absorption of an ultraviolet (second-harmonic) photon. Since these states lie at energies more than 2/3 of the way to the ionization limit, absorption of one ultraviolet (second-harmonic) photon to excited the state, followed by absorption of a visible (fundamental) photon leading to photoionization was found to be a very efficient process. The much greater intensity of the fundamental radiation as compared to the ultraviolet insured that a high fraction of the molecules which were excited by the absorption of an ultraviolet photon would be ionized as well. This led to strong features in the low-resolution spectra of AlAr and AlKr and permitted observation of transitions that correlate to electric dipole forbidden transitions in the isolated aluminum atom.

Spectroscopic features were detected by monitoring mass 67 ($AlAr^+$) for scans of AlAr, but some band systems (particularly at higher energies) were found at mass 27 (Al^+) as well. These banded features occurring at the mass of (Al^+) must of course correspond to excitation of the AlAr complex, which then dissociates to give a strong Al^+ signal. Accordingly, mass 27 was monitored along with mass 67 in the AlAr experiments. In the AlKr experiments the major isotopic modifications were separately monitored at mass 109 ($^{27}Al\ ^{82}Kr$, 11.6%), 110 ($^{27}Al\ ^{83}Kr$, 11.5%), 111 ($^{27}Al\ ^{84}Kr$, 57.0%), and 113 ($^{27}Al\ ^{86}Kr$, 17.3%). Although the AlKr complex also displayed a tendency toward dissociation, with spectral features occurring at the mass of the Al^+ ion, monitoring of the Al^+ signal was complicated since the 5% krypton in argon carrier gas also generated a few AlAr molecules. As a result, the signal at mass 27 was a combination of true transitions in aluminum atoms (which were easily identified using Moore's tables[22]), transitions in AlAr which led to Al^+ products, and transitions in AlKr (in all of its isotopic modifications) which led to Al^+ products. With all of these processes occurring in a congested spectral region, care was required in the assignment of band systems observed in the Al^+ channel to AlKr.

Absolute frequency calibrations were obtained from the transitions occurring in atomic aluminum.[22] Below 40 000 cm^{-1} calibrations were also obtained by narrowing the linewidth of the pulsed dye laser by the insertion of an air-spaced intracavity étalon, and pressure tuning with SF_6. An absorption spectrum of gaseous I_2 was then simultaneously collected along with a scan over a particular vibronic band of AlKr, allowing an absolute calibration to be made with the aid of the I_2 atlas.[23] In this calibration the Doppler shift experienced by the AlAr and AlKr molecules as they traveled toward the radiation source was taken into account, although it amounted to less than 0.3 cm^{-1} for all of the observed transitions. With these two calibration methods, we believe that our reported band positions are accurate to within $\pm 1\ cm^{-1}$ in most cases, and to within $\pm 3\ cm^{-1}$ at worst.

Unlike the studies of molecules such as CuAg,[24] CuAu,[25] NiPt,[26] etc. reported from this group, the AlAr and AlKr molecules were not investigated with rotational resolution. The rotational structure of AlAr and AlKr is considerably more complex than that of the intermetallic diatomics cited above, and could not be adequately resolved with the 0.06 cm^{-1} laser bandwidth available in the present experiments using frequency-doubled dyes. A few of the bands observed for AlKr were investigated at 0.06 cm^{-1} resolution, however, with the goal of accurately measuring the splitting between the various isotopic modifications, so that an absolute vibrational assignment could be obtained.

III. RESULTS

A. Ionization potentials

1. AlAr, $AlAr_2$, and $AlAr_3$

Figure 1 displays the recorded ion signals of Al^+, $AlAr^+$, $AlAr_2^+$, and $AlAr_3^+$ which were obtained as the dye

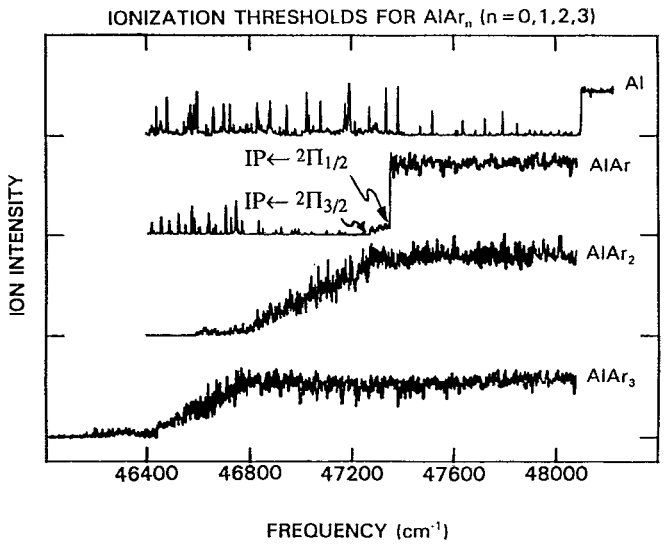

FIG. 1. The one-photon ionization thresholds of Al, AlAr, $AlAr_2$, and $AlAr_3$, recorded in an electrostatic field of approximately 141 V/cm, using frequency-doubled stilbene 420 laser dye.

laser was scanned over the range from 46 000 to 48 400 cm^{-1}. The onset of a one-photon ionization process is evident in atomic aluminum as a step function rise in ion signal at 48 090.5 cm^{-1}. This is significantly less than the known ionization potential of ground-state aluminum atoms, which has been accurately measured to be 48 278.480 $\pm$ 0.003 cm^{-1}.[19] Two factors contribute to this difference: First, a population of spin–orbit excited $3s^23p^1, {}^2P^0_{3/2}$ aluminum atoms is present in the jet-cooled molecular beam, and this state lies 112.04 cm^{-1} above the $3s^23p^1, {}^2P^0_{1/2}$ ground state.[22] The large increase in Al^+ ion signal observed at 48 090.5 cm^{-1} corresponds to the direct, one-photon ionization of aluminum atoms in the spin–orbit excited $^2P^0_{3/2}$ state.

A second contributing factor arises because the experiments are conducted in an electrostatic field, which lowers the apparent ionization potential due to field-ionization effects. The magnitude of this effect can be calculated assuming a $-e^2/r$ attraction of a Rydberg electron toward a positively charged core.[27–29] In the presence of a uniform electrostatic field in the z direction, E_z, however, an additional term must be added to this potential, given by $E_z ez$. The total potential is then given as $V = -e^2/r + E_z ez$. An electron moving in this potential can tunnel through the barrier, resulting in field ionization. In addition, however, electrons having an energy greater than $-2e(eE_z)^{1/2}$ lie above the barrier to ionization, and may leave the atom *without* tunneling through a barrier. As a result, the apparent ionization potential of an atom or molecule in an electric field of strength E_z is reduced by $2e(eE_z)^{1/2}$ from the field-free value. For a field E_z given in V/cm, this results in a shift of the ionization threshold (given in wave numbers, cm^{-1}) of $-6.1215E_z^{1/2}$. In the experiments reported here an electric field of approximately 141 V/cm was used, corresponding to a field-ionization shift of -72.8 cm^{-1}. This shift, applied to the ionization potential of a $^2P^0_{3/2}$ aluminum atom, leads to a predicted apparent ionization threshold of 48 093.64 cm^{-1}, in good agreement with the observed value of 48 090.5 cm^{-1}.

The ion signal displayed in Fig. 1 for AlAr exhibits an apparent one-photon ionization threshold at 47 342.6 cm^{-1}. Correcting this value by the experimentally measured field-ionization shift found for the $^2P^0_{3/2}$ state of atomic aluminum (75.9 cm^{-1}) results in an adiabatic ionization potential of 47 418.5 $\pm$ 2 cm^{-1} (5.8791 $\pm$ 0.0002 eV) for AlAr. This represents a shift of 860.0 $\pm$ 2 cm^{-1} from the ionization potential of ground-state aluminum atoms, and reflects an increased stability of the $AlAr^+$ cation over the AlAr neutral by this amount.

In addition to the strong onset of one-photon ionization observed for AlAr at 47 342.6 cm^{-1}, a much weaker continuous absorption is observed extending further to the red, ending abruptly at 47 261.7 cm^{-1}. Three explanations for this feature are possible: First, it might correspond to a small population of vibrationally excited ($v'' = 1$) AlAr molecules, which would require less energy for photoionization than is required by molecules with $v'' = 0$. If this were the case, the energy difference between the two thresholds (80.9 $\pm$ 2 cm^{-1}) would correspond to the value of $\Delta G''_{1/2}$ for the AlAr ground state. This has been measured in dispersed fluorescence studies by Callender, Mitchell, and Hackett, however, and is found to be approximately 30 cm^{-1}.[13] Accordingly, this possibility is dropped from further consideration.

A second possibility is that there are poor Franck–Condon factors for accessing the $AlAr^+$ $v = 0$ level, and that the weak threshold corresponds to an ionization process forming $AlAr^+$ in $v = 0$, and the stronger threshold corresponds to formation of $AlAr^+$ in $v = 1$. This would require that the value of $\Delta G''_{1/2}$ for the $AlAr^+$ *ion* be 80.9 $\pm$ 2 cm^{-1}. Although this is certainly possible, the large disparity in intensity of the two thresholds argues against this interpretation. Indeed, the stronger threshold is not accurately represented in Fig. 1, since the detection system is fully saturated for $AlAr^+$ in the high-frequency range of Fig. 1. The stronger threshold corresponds to an ionization efficiency which is *at least* a factor of 10 greater than that observed for the weaker threshold. It seems unlikely that the Franck–Condon factors for the direct one-photon ionization process would increase by more than a factor of 10 in going from the 0–0 to 1–0 excitations. Therefore this possibility is dropped from consideration as well.

A third possibility is that there is a small population of spin–orbit excited $X_2\,{}^2\Pi_{3/2}(3p)$ states in our molecular beam, and that the separation between the two thresholds is indicative of the energy difference between the $X_1\,{}^2\Pi_{1/2}(3p)$ and $X_2\,{}^2\Pi_{3/2}(3p)$ levels. Assuming a pure π^1 configuration for the ground state of AlAr, with the π molecular orbital localized as an unperturbed aluminum $3p\pi$ orbital, the expected spin–orbit splitting is given by $\zeta_{3p}(\mathrm{Al})$, listed by Lefebvre-Brion and Field[30] as 74.7 cm^{-1}. Our value of 80.9 $\pm$ 2 cm^{-1} is in good agreement with this result, and is in excellent agreement with the value of 79.8 $\pm$ 5 cm^{-1} obtained in dispersed fluorescence studies by Callender,

Mitchell, and Hackett.[13] Accordingly, we assign the two thresholds observed in Fig. 1 to the direct, one-photon ionization thresholds for $X_2\ ^2\Pi_{3/2}(3p)$ and $X_1\ ^2\Pi_{1/2}(3p)$ AlAr, respectively.

Figure 1 also displays the ionization threshold for $AlAr_2$ and $AlAr_3$. These exhibit gradual onsets rather than the abrupt increases found for atomic aluminum and AlAr. Evidently, these species undergo serious geometrical rearrangements upon ionization, making the Franck–Condon factors for excitation to the vibrationless level of the ionic ground state very poor indeed. Nevertheless, a sudden increase in ion signal from a nearly zero base line is obvious for $AlAr_2$ at $46\,584.4 \pm 2\ cm^{-1}$. After correcting for the field-ionization shift ($75.9\ cm^{-1}$) this brings the adiabatic ionization potential for $AlAr_2$ to $46\,660.3 \pm 2\ cm^{-1}$ (5.7851 ± 0.0002 eV). For the $AlAr_3$ complex an unambiguous assignment of the adiabatic ionization potential is not possible, but a definite increase in base-line noise near $46\,219\ cm^{-1}$ may correspond to the one-phonon ionization threshold. After correcting for the field-ionization shift ($75.9\ cm^{-1}$), this gives an estimated adiabatic ionization potential for $AlAr_3$ of $46\,295\ cm^{-1}$ (5.7399 eV).

These results show a shift in the ionization threshold of aluminum as argon atoms are sequentially added. Moreover, the shifts are nearly constant as the first two argon atoms are added, at 0.1067 eV [IP(Al)-IP(AlAr)] and 0.0940 eV [IP(AlAr)-IP($AlAr_2$)]. The third argon atom appears to have a somewhat lesser effect, giving an ionization potential shift of 0.0452 eV [IP($AlAr_2$)-IP($AlAr_3$)]. These results would seem to indicate that the first two argon atoms interact nearly equally well with the Al^+ ion, but that the third is somewhat shielded from the bare ion by the other two argon atoms.

2. AlKr

Figure 2 displays the analogous scan over the ionization threshold of AlKr, which was recorded at somewhat reduced laser fluence as compared with the AlAr spectrum. (This was inadvertent, due to serious damage which had been accidentally inflicted upon the BBO frequency-doubling crystal.) Above $46\,868.8\ cm^{-1}$ an intense structured spectrum is observed, while below this frequency much weaker transitions may be seen. The abrupt onset of the intense structured spectrum is assigned as the threshold of a one-photon ionization process, while the much weaker transitions are assigned to high Rydberg levels lying below the ionization limit, which require the absorption of a second photon for ionization to occur. Applying the field-ionization correction of $75.9\ cm^{-1}$ to the measured threshold frequency of $46\,868.8 \pm 2\ cm^{-1}$ gives an adiabatic ionization potential of $46\,944.7 \pm 2\ cm^{-1}$ (5.8204 ± 0.0002 eV) for AlKr.

Perhaps the most troubling aspect of this interpretation lies in the discrete nature of the intense transitions above the assigned ionization limit. As is discussed more fully in the descriptions of the individual band systems below, there are severe Franck–Condon problems in accessing the $v' = 0$ levels of the strongly bound Rydberg states in the AlKr complex. In the $^2\Delta(6d) \leftarrow X_1\ ^2\Pi_{1/2}(3p)$ system, for example, the first observed band is the 2–0 band. One would expect that a direct excitation to the $v' = 0$ level of the $AlKr^+$ ion would exhibit similar Franck–Condon difficulties. Accordingly, we propose that the intense structured features in the spectrum of Fig. 2 correspond to excitation of excited vibrational levels ($v' \geqslant 2$) of high Rydberg states of the AlKr complex, which lie above the $v' = 0$ level of the $AlKr^+$ ion. In such cases vibrational autoionization can efficiently ionize the complex, so that absorption of a second photon is not required. Of course, the resulting spectrum is highly structured, since it displays the vibrational structure of the high Rydberg states, which appears to be broadened by the rapid autoionization process. This phenomenon of vibrational autoionization was not so apparent in our studies of AlAr (Fig. 1), because the greater laser fluence that was available prior to damaging the BBO crystal led to a saturation of the detection system above the one-photon ionization threshold.

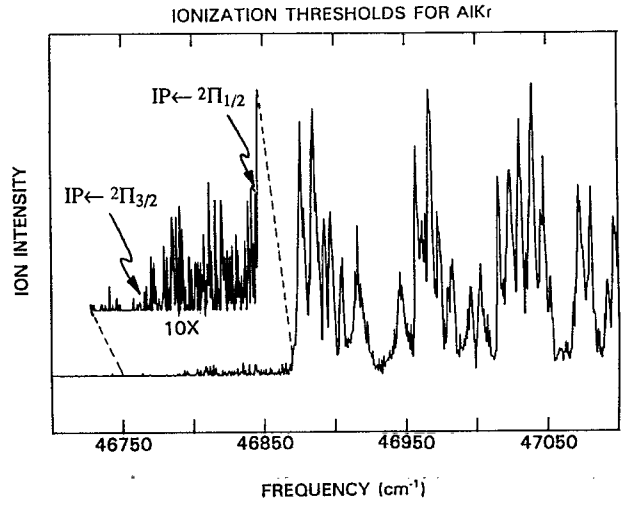

FIG. 2. The one-photon ionization threshold of $^{27}Al\ ^{84}Kr$, recorded in an electrostatic field of approximately 141 V/cm.

Figure 2 also shows a blown-up view of the region immediately below the one-photon ionization threshold. Here another near-continuum absorption is found, beginning at $46\,790.4 \pm 3\ cm^{-1}$. It is much weaker in intensity than the near-continuum which begins at $46\,868.8\ cm^{-1}$, but appears otherwise similar. As in the case of AlAr, we interpret this underlying weak continuum as arising from the direct one-photon ionization of $X_2\ ^2\Pi_{3/2}(3p)$ spin–orbit excited states of the AlKr complex, which are very slightly populated in the jet-cooled molecular beam. Adding the field-ionization shift measured for the aluminum atom ($75.9\ cm^{-1}$) to the measured threshold, we obtain an adiabatic ionization potential for the $X_2\ ^2\Pi_{3/2}(3p)$ state of AlKr of $46\,866.3 \pm 3\ cm^{-1}$. This then allows the spin-orbit splitting of the ground $X\ ^2\Pi(3p)$ state of AlKr to be estimated as $78.4 \pm 4\ cm^{-1}$, in uncanny agreement with the value of $78.4 \pm 5\ cm^{-1}$ obtained in a dispersed fluorescence study by Callender, Mitchell, and Hackett.[13]

B. The $3d \leftarrow 3p$ excitation and the bond strengths of AlAr and AlKr

1. AlKr

Figure 3 displays the band spectra obtained in the $^{27}Al\,^{84}Kr$ mass channel when the frequency-doubled dye laser was scanned over the 31 600–32 700 cm^{-1} range. This is close to the fully allowed $3s^23d^1$, $^2D_{3/2,5/2} \leftarrow 3s^23p^1$, $^2P^0_{1/2}$ transitions of atomic aluminum at 32 435.45 and 32 436.79 cm^{-1}.[22] In addition, the $3s^24p^1$, $^2P^0_{1/2,3/2} \leftarrow 3s^23p^1$, $^2P^0_{1/2}$ transitions of atomic aluminum would be expected at 32 949.84 and 32 965.67 cm^{-1} if they were not forbidden under electric dipole selection rules.[22] At the long-wavelength end of the region displayed in Fig. 3 the spectrum is dominated by a regular progression of blue-shaded bands which display an unusual intensity pattern. These bands have been recorded at 0.06 cm^{-1} resolution, which was insufficient for a complete rotational analysis. Nevertheless, absolute band frequencies have been determined using the I_2 atlas for calibration, and isotope shifts between the $^{27}Al\,^{82}Kr$ and $^{27}Al\,^{86}Kr$ isotopic modifications have been used to establish an absolute vibrational numbering. Calculated and measured isotope shifts are compared for three different vibrational numberings in Fig. 4, clearly establishing that a correct absolute vibrational numbering has been obtained. Tables of the measured band positions and isotopic shifts for all of the band systems reported in this article for both AlAr and AlKr are available from the Physics Auxiliary Publication Service (PAPS) of the American Institute of Physics or from one of the authors (M.D.M.).[31]

The $3s^23d^1, ^2D \leftarrow 3s^23p^1\,^2P^0$ transition of atomic aluminum is expected to split into $^2\Sigma^+(3d) \leftarrow X_1\,^2\Pi_{1/2}(3p)$, $^2\Pi(3d) \leftarrow X_1\,^2\Pi_{1/2}(3p)$, and $^2\Delta(3d) \leftarrow X_1\,^2\Pi_{1/2}(3p)$ transitions when the symmetry of the system is reduced from the full spherical symmetry of the atom to $C_{\infty v}$ symmetry in AlKr, and only transitions originating from the $X_1\,^2\Pi_{1/2}(3p)$ ground state are considered. Just as the $^2\Sigma^+(3p)$ state lies at a much higher energy than the $X_1\,^2\Pi_{1/2}(3p)$ ground state, owing to an unfavorable interaction between the $3p\sigma$ orbital of aluminum and the krypton atom, we expect the $^2\Sigma^+(3d)$ state to lie considerably higher in energy than either the $^2\Pi(3d)$ or $^2\Delta(3d)$ states of AlKr. In addition, the $^2\Delta(3d)$ state of AlKr places the electron density of the $3d$ electron farther from the krypton atom than does the $^2\Pi(3d)$ state, allowing the krypton atom to approach the aluminum more closely and interact more strongly. This probably makes the $^2\Delta(3d)$ state of AlKr the most strongly bound of the states correlating to the $3s^23d^1, ^2D(Al) + {}^1S_0(Kr)$ separated atom limit. This fundamental picture has also been obtained in theoretical calculations of the interaction of an electronically excited $3s^13d^1, {}^1D$ or ^3D magnesium atom with argon, resulting in the energetic ordering of the electronic states of $^1\Delta < {}^1\Pi < {}^1\Sigma^+$, and $^3\Delta < {}^3\Pi < {}^3\Sigma^+$, respectively.[32] With this in mind, the regular progression displayed at the low-frequency end of Fig. 3 is assigned as the $^2\Delta(3d) \leftarrow X_1\,^2\Pi_{1/2}(3p)$ excitation of AlKr.

The $^2\Delta(3d) \leftarrow X_1\,^2\Pi_{1/2}(3p)$ band system of AlKr displays an unusual intensity pattern, with the 6–0, 9–0, and 10–0 bands at 31 948, 32 129, and 32 183 cm^{-1} much more intense than can be explained on the basis of Franck–Condon arguments. A similar intensity anomaly is found for the analogous band system of AlAr, in which one band (at 32 095 cm^{-1}) is much more intense than all others combined (see below). Our detection scheme is based upon photoionization rather than fluorescence, so it is possible that the anomalous intensity pattern results from anomalies in the ionization step. A key to understanding this unusual pattern can be found by considering the total energy available to the molecule from the combination of excitation and ionization photons.

The combined energy of the second-harmonic radiation (which is responsible for excitation) and the fundamental radiation (which is much more intense and is primarily responsible for ionization) for these anomalous bands falls in the range of 47 922–48 275 cm^{-1} for AlKr and falls at 48 142 cm^{-1} for AlAr. This total is barely enough to ionize the molecules, which have ionization potentials of

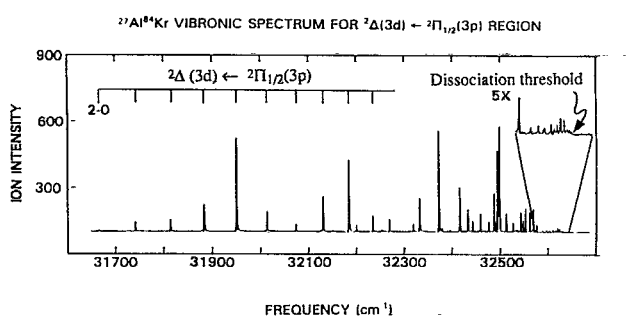

FIG. 3. The R2PI spectrum of the 31 600–32 700 cm^{-1} region of $^{27}Al\,^{84}Kr$, in which the $3d \leftarrow 3p$ excitation is expected, scanned using frequency-doubled DCM and DCM/rhodamine 640 laser dyes. Convergence to the $3s^23d^1, {}^2D(Al) + {}^1S_0(Kr)$ separated atom limit (shown in greater detail in the expanded inset) is used to assign the bond strength of the ground $X_1\,^2\Pi_{1/2}(3p)$ state.

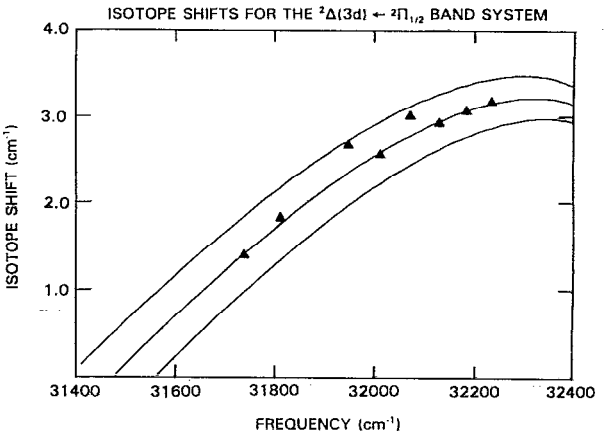

FIG. 4. Measured isotope shifts $[\nu(^{27}Al\,^{82}Kr) - \nu(^{27}Al^{86}Kr)]$ as a function of transition frequency, along with calculated isotope shifts for three different vibrational numberings of the $^2\Delta(3d) \leftarrow X_1\,^2\Pi_{1/2}(3p)$ system. The middle curve corresponds to the numbering shown in Fig. 3, which is most probably correct.

46 944.7 ± 2 and 47 418.5 ± 2 cm^{-1} for AlKr and AlAr, respectively. Moreover, the ground-state bond strengths (derived below as 194.7 and 122.4 cm^{-1} for AlKr and AlAr, respectively) may be combined with the ionization potential of atomic aluminum (48 278.480 cm^{-1})[19] to give the energies of the separated atom limits $Al^+ + (Kr,Ar) + e^-$ above the $X_1\,^2\Pi_{1/2}(3p), v'' = 0$ level as 48 473.2 and 48 400.9 cm^{-1} for AlKr and AlAr, respectively. Thus, in both molecules bands with anomalous intensity fall in the energy range where the sum of the second harmonic and fundamental photon energies is sufficient to ionize the molecule, but cannot ionize *and* dissociate the molecule. In this range there is a large density of electronic states because of the nesting of Rydberg states as one approaches the ionization limit. The anomalous intensities probably result because of accidental resonances in the ionization step, in which the ionization photon excites the molecule to an excited vibrational level of a high Rydberg state, as schematically illustrated in Fig. 5. Since the total energy lies above the ground vibrational level of the ion, autoionization can occur by nonadiabatic coupling to the ionic ground electronic state, resulting in formation of $AlKr^+$ or $AlAr^+$. This proposed mechanism explains the unusual intensity pattern,

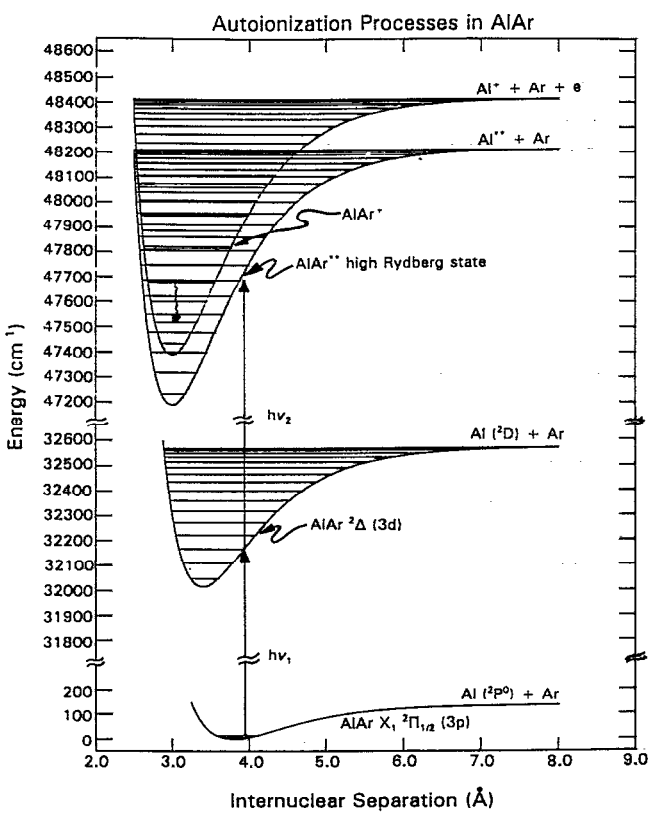

FIG. 5. An autoionization mechanism for the unusual intensity pattern in the $^2\Delta(3d) \leftarrow X_1\,^2\Pi_{1/2}(3p)$ band system of AlAr and AlKr. This band system is located at almost precisely 2/3 of the ionization energy, so that the combination of one ultraviolet photon to excite the system to the $^2\Delta(3d)$ state, and one visible photon (at half of the frequency of the UV photon) can ionize the molecule, but does not have sufficient energy to ionize and fragment the molecule. See the text for further details.

because the Franck–Condon factor for excitation to a high vibrational level of a high Rydberg state may be much greater than the Franck–Condon factor for excitation directly into the ionization continuum, where only the lower vibrational levels of the ion are energetically accessible. Efficient nonadiabatic coupling to the ionization continuum can then ionize these vibrationally excited high Rydberg states with nearly unit probability, leading to greatly enhanced ion signals. The random pattern of strong transitions then results from an accidental pattern of resonances in the ionization step. Of course, precise accidental resonances would only be expected for specific J levels, but the laser bandwidths of the UV and visible radiation in this low-resolution scan ($\approx$1.5 and $\approx$0.7 cm^{-1}, respectively) relax this constraint considerably, allowing entire bands to show intensity anomalies. Rotational level broadening in the autoionizing high Rydberg state also contributes to a relaxation of this constraint.

In addition to the regular progression assigned to the $^2\Delta(3d) \leftarrow X_1\,^2\Pi_{1/2}(3p)$ band system, Fig. 3 also displays a complicated set of features further to the blue, which become more congested until a limit is reached. Indeed, this set of features is far more complicated than one would expect for a set of only three overlapping band systems described as the $^2\Delta(3d) \leftarrow X_1\,^2\Pi_{1/2}(3p)$, $^2\Pi(3d) \leftarrow X_1\,^2\Pi_{1/2}(3p)$, and $^2\Sigma^+(3d) \leftarrow X_1\,^2\Pi_{1/2}(3p)$ systems. For this reason we believe that the nearby $^2\Pi(4p) \leftarrow X_1\,^2\Pi_{1/2}(3p)$ and $^2\Sigma^+(4p) \leftarrow X_1\,^2\Pi_{1/2}(3p)$ band systems, which are electric dipole forbidden in the isolated aluminum atom, gain intensity by mixing with the corresponding $^2\Pi(3d) \leftarrow X_1\,^2\Pi_{1/2}(3p)$ and $^2\Sigma^+(3d) \leftarrow X_1\,^2\Pi_{1/2}(3p)$ systems. Since the atomic $^2P^0_{1/2}(4p)$ state lies only 514 cm^{-1} above the $^2D_{3/2}(3d)$ state,[22] it is likely that the $^2\Pi(4p)$ and $^2\Sigma^+(4p)$ potential curves drop into the energy range scanned in Fig. 3, introducing extraneous vibrational features which make the detailed assignment of the spectrum difficult. Although fragments of other band systems have been tentatively identified in the spectrum of Fig. 3, the most useful piece of information which may be obtained from this spectrum is the bond strength of the $^{27}Al\,^{84}Kr$ molecule in its $X_1\,^2\Pi_{1/2}(3p)$ ground state. This may be determined from the convergence limit of the closely spaced bands at the high-frequency end of the spectrum, which is clearly seen at 32 630.1 cm^{-1}. This limit can only correspond to the production of $Al(3s^23d\,^1,^2D) + Kr(^1S_0)$, since it lies to the red of the forbidden atomic $^2P^0_{1/2}(4p) \leftarrow {}^2P^0_{1/2}(3p)$ transition, calculated to occur at 32 949.84 cm^{-1}.[22] With this information in hand, the ground-state binding energy of $^{27}Al\,^{84}Kr$ may be derived as $D_0(^{27}Al\,^{84}Kr) = 194.7 \pm 0.8$ cm^{-1}, where the error limit is taken as the energy difference between the last two observed bands, and it is assumed that dissociation occurs at the $^2D_{3/2} + {}^1S_0$ separated atom limit (at 32 435.45 cm^{-1}).[22] Since the spin–orbit splitting between the $^2D_{3/2}$ and $^2D_{5/2}$ spin–orbit components of the $3s^23d^1$ configuration of atomic aluminum is only 1.34 cm^{-1},[22] this last assumption is of minor consequence, and the binding energy is probably determined to within 1 cm^{-1}. We note that this value [$D_0(^{27}Al\,^{84}Kr = 194.7 \pm 0.8$ cm^{-1}] lies well within the uncertainty limits of the only

previous estimate, given by Callender, Mitchell, and Hackett[13] as $D_0(\mathrm{AlKr}) = 181 \pm 68\ \mathrm{cm}^{-1}$.

With the ionization potential of AlKr accurately determined to be $46\,944.7 \pm 2\ \mathrm{cm}^{-1}$ and the binding energy of the ground state now determined as $D_0(\mathrm{AlKr}) = 194.7 \pm 0.8\ \mathrm{cm}^{-1}$, the binding energy of the ion may be determined through the thermodynamic cycle

$$D_0(\mathrm{Al}^+\text{–Kr}) = D_0(\mathrm{AlKr}) + \mathrm{IP(Al)} - \mathrm{IP(AlKr)}\,. \tag{3.1}$$

Combination of our results with the known ionization potential of atomic aluminum ($48\,278.480 \pm 0.003\ \mathrm{cm}^{-1}$)[19] then gives the binding energy of AlKr^+ as $D_0(\mathrm{Al}^+\text{–Kr}) = 1528.5 \pm 2\ \mathrm{cm}^{-1}$.

2. AlAr

Figure 6 displays the resonant two-photon ionization spectrum of AlAr in the region of the $3d \leftarrow 3p$ transition, which is analogous to Fig. 3 for AlKr. Again, a regular progression with an unusual intensity pattern is observed at the long-wavelength end of the spectrum. In this case the second observed band, at $32\,095\ \mathrm{cm}^{-1}$, is far more intense than any other feature in the progression. As was invoked for AlKr above, it is thought that this anomalous intensity pattern results from an accidental resonance with an autoionizing state at an energy of $48\,142\ \mathrm{cm}^{-1}$.

This lowest energy band system associated with the $3d \leftarrow 3p$ transition is again assigned as the $^2\Delta(3d) \leftarrow X_1\,^2\Pi_{1/2}(3p)$ system, and band positions are available from the Physics Auxiliary Publication Service (PAPS) of the American Institute of Physics or from one of the authors (M.D.M.).[31] Unfortunately, in the case of AlAr both elements possess only one major isotope (in greater than 99% natural abundance), so no isotopic shift information is available to assist in obtaining an absolute vibrational numbering. The numbering given in Fig. 6 is based on a knowledge of the bond strength of AlAr^+ (see below), which is thought to be an upper limit on the bond strength of all of the electronic states of the neutral complex. In addition, the vibrational numbering chosen for this and the other $^2\Delta(nd)$ band systems has been selected so that the bond strengths of the $^2\Delta(nd)$ states of AlAr increase uniformly (within a few cm^{-1}) as n increases. Even with these constraints, it is possible that the correct numbering of the first observed band of the $^2\Delta(3d)$ system may be as the 0–0, 1–0, 2–0, or 3–0 band. However, these same constraints applied to the $^2\Delta(4d) \leftarrow X_1\,^2\Pi_{1/2}(3p)$ system (see below) show that the 0–0 band is indeed observed in this instance. Since a greater shift in equilibrium internuclear separation is expected in the $^2\Delta(4d) \leftarrow X_1\,^2\Pi_{1/2}(3p)$ system than in the $^2\Delta(3d) \leftarrow X_1\,^2\Pi_{1/2}(3p)$ system, we therefore feel confident that the first observed band in the $^2\Delta(3d) \leftarrow X_1\,^2\Pi_{1/2}(3p)$ system is the 0–0 band as well. Indeed, we believe that the 0–0 band is observed in all of the $^2\Delta(nd) \leftarrow X_1\,^2\Pi_{1/2}(3p)$ band systems which we have analyzed ($n = 3$–9), with the sole exception of the $^2\Delta(9d)$ Rydberg state. This is in marked contrast with the results for AlKr, where isotope shift measurements indicate that 0–0 bands are frequently too weak to be observed.

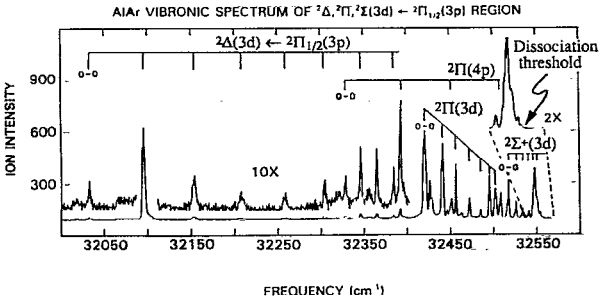

FIG. 6. The 32 000–32 600 cm^{-1} spectral region of AlAr, in which the $3d \leftarrow 3p$ transition is expected. As was found for AlKr, convergence to the $3s^2 3d\,^1,^2D + {}^1S_0$ separated atom limit is observed in the expanded inset at 32 557.8 cm^{-1}, allowing the bond strength of the $X_1\,^2\Pi_{1/2}(3p)$ ground state to be accurately measured.

Above 32 320 cm^{-1} the spectrum shown in Fig. 6 for AlAr becomes quite complicated, just as occurred in AlKr. However, a strong apparent origin band is evident at 32 421 cm^{-1}, followed by a regular progression of bands of diminishing intensity. This is assigned as the $^2\Pi(3d) \leftarrow X_1\,^2\Pi_{1/2}(3p)$ system, based on the idea that in the $3s^2 nd\,^1$ states of aluminum, the ordering of electronic states is $^2\Delta(nd) < {}^2\Pi(nd) < {}^2\Sigma^+(nd)$. A list of band positions is available from the Physics Auxiliary Publication Service (PAPS) of the American Institute of Physics or from one of the authors (M.D.M.).[31]

A much weaker progression is also labeled in Fig. 6, beginning about 93 cm^{-1} to the red of the origin band of the $^2\Pi(3d) \leftarrow X_1\,^2\Pi_{1/2}(3p)$ system. These bands are quite weak below 32 400 cm^{-1}, but become more intense in the congested region to the blue of the origin of the $^2\Pi(3d) \leftarrow X_1\,^2\Pi_{1/2}(3p)$ system. According to our ideas about the energetic ordering of the $^2\Delta(3d)$, $^2\Pi(3d)$, and $^2\Sigma^+(3d)$ states, this system cannot correspond to the $^2\Sigma^+(3d) \leftarrow X_1\,^2\Pi_{1/2}(3p)$ system, which is expected to the blue of the $^2\Pi(3d) \leftarrow X_1\,^2\Pi_{1/2}(3p)$ system. Accordingly, it is assigned as correlating to the $3s^2 4p^1, {}^2P^0 \leftarrow 3s^2 3p^1, {}^2P^0$ transition, which is forbidden under electric dipole selection rules in atomic aluminum. Presumably, this is the $^2\Pi_{1/2}(4p) \leftarrow X_1\,^2\Pi_{1/2}(3p)$ band system, which gains intensity by its proximity to the fully allowed $^2\Pi(3d) \leftarrow X_1\,^2\Pi_{1/2}(3p)$ system. A list of band positions is available from the Physics Auxiliary Publication Service (PAPS) of the American Institute of Physics or from one of the authors (M.D.M.).[31]

Finally, another series of bands is present at the high-frequency end of the spectrum presented in Fig. 6. Beginning at 32 517 cm^{-1}, it is unclear whether these bands represent the $^2\Sigma^+(3d) \leftarrow X_1\,^2\Pi_{1/2}(3p)$ system or are simply transitions to high vibrational levels of the $^2\Delta(3d)$ and/or $^2\Pi(3d)$ systems. In any case, these are labeled in Fig. 6 as the $^2\Sigma^+(3d) \leftarrow X_1\,^2\Pi_{1/2}(3p)$ system. A list of band positions is available from the Physics Auxiliary Publication Service (PAPS) of the American Institute of Physics or from one of the authors (M.D.M.).[31]

As was the case for AlKr, the most useful information which may be derived from this spectrum is the observation of a convergence limit, defined by the last observed band at 32 557.8 cm^{-1}. Assuming this represents the dissociation limit for production of a $3s^2 3d\,^1, {}^2D_{3/2}$ aluminum atom and a ground-state argon atom, this places the bond strength of the ground state of AlAr at $D_0[\mathrm{AlAr}, X_1\,{}^2\Pi_{1/2}(3p)] = 122.4$ cm^{-1}. Given that the last few bands of the purported $^2\Sigma^+(3d) \leftarrow X_1\,{}^2\Pi_{1/2}(3p)$ system overlap, resulting in the broadened feature which is the last discernible transition in Fig. 6, it seems that this limit is defined to within approximately ± 4 cm^{-1}, giving $D_0[\mathrm{AlAr}, X_1\,{}^2\Pi_{1/2}(3p)] = 122.4 \pm 4$ cm^{-1}. With the ionization potential of AlAr accurately determined to be $47\,418.5 \pm 2$ cm^{-1} and the binding energy of the ground state now determined, the binding energy of the cation may be determined through a thermodynamic cycle analogous to Eq. (3.1), giving $D_0(\mathrm{Al}^+\text{–Ar}) = 982.3 \pm 5$ cm^{-1}.

This measurement of the binding energy of AlAr is somewhat at odds with previous estimates of $D_0[\mathrm{AlAr}, X_1\,{}^2\Pi_{1/2}(3p)]$, given as $\geqslant 133$,[12] 136 ± 65,[13] and 165^{+40}_{-10} cm^{-1}.[15] While one could imagine that our measured bond strength, which is based on observing the convergence limit of a set of vibrational levels, could be erroneously *high* due to a barrier in the potential-energy curve, it is difficult to understand how such a method could give an erroneously *low* value. On the other hand, the estimates of ($D_0 \geqslant 133$ cm^{-1}) (Ref. 12) and (155 $cm^{-1} \leqslant D_0 \leqslant 205$ cm^{-1}) (Ref. 15) are based on an analysis of the $B\,{}^2\Sigma^+(4s) \leftarrow X_1\,{}^2\Pi_{1/2}(3p)$ band system and the thermodynamic cycle

$$D_0(X_1) = \nu_{00} + D_0(B) - \nu_{\mathrm{atomic}}, \tag{3.2}$$

where $D_0(X_1)$ and $D_0(B)$ are the bond strengths of the $X_1\,{}^2\Pi_{1/2}(3p)$ and $B\,{}^2\Sigma^+(4s)$ states, respectively, ν_{00} is the frequency of the 0–0 band of the B–X_1 system, and ν_{atomic} is the frequency of the $3s^2 4s^1, {}^2S_{1/2} \leftarrow 3s^2 3p^1, {}^2P^0_{1/2}$ atomic transitions. Since ν_{atomic} is very well known, only the remaining terms need to be examined as potential sources of error. The bond strength of the $X_1\,{}^2\Pi_{1/2}(3p)$ state could have been overestimated in previous studies if either ν_{00} or $D_0(B)$ were overestimated. A possible source of error in ν_{00} could be an erroneous vibrational numbering of the B–X_1 system, so that the true value of ν_{00} would lie below that used in Eq. (3.2). This possibility seems unlikely, however, since the Franck–Condon factors for the $B\,{}^2\Sigma^+(4s)$, $v' \leftarrow X_1\,{}^2\Pi_{1/2}(3p)$, $v'' = 0$ transitions ($v' = 1$–7), calculated from a potential based on a Rydberg–Klein–Rees (RKR) analysis of the vibrational and rotational constants, are in excellent agreement with experiment.[15]

The only remaining potential source of error in Eq. (3.2) lies in the value of $D_0(B)$. However, the lower limits quoted by Gardner and Lester ($D_0 \geqslant 133$ cm^{-1})[12] and McQuaid, Gole, and Heaven ($D_0 \geqslant 155$ cm^{-1}), are based on the inequality $D_0(B) \geqslant \nu_{v'-0} - \nu_{0-0}$, where $\nu_{v'-0}$ and ν_{0-0} are the frequencies of the v'–0 and 0–0 bands, respectively. At first glance, this inequality would seem to be obviously true, but it will be in error if the potential-energy curve of the $B\,{}^2\Sigma^+(4s)$ state possesses a barrier to dissociation, so that quasibound vibrational levels may exist *above* the energy of the separated $3s^2 4s^1, {}^2S_{1/2}\mathrm{Al} + {}^1S_0$ Ar atoms. Such vibrational levels will of course undergo predissociation by tunneling through the barrier, but if this rate is slow compared to fluorescence the predissociation quantum yield will be small and would not be obvious in laser-induced fluorescence experiments.

A barrier to dissociation in the $B\,{}^2\Sigma^+(4s)$ state of AlAr should not be unexpected, since such effects have been previously observed in the $C,D\,{}^3\Sigma^+(6s^1 7s^1)$ state of HgAr,[33] which is similar to the $^2\Sigma^+(4s)$ state of AlAr in the sense that one electron has been promoted to the first s-type Rydberg orbital. At very long range the interaction between the two atoms is attractive because of long-range $1/R^6$ dispersion forces, but at shorter distances a repulsion will set in as the argon atom encounters the s Rydberg electron. At even shorter range, however, Duval *et al.* suggest that the argon can penetrate into the diffuse 7s orbital, where it interacts strongly with the Hg^+ ion core.[33] This results in a double minimum potential, which is found to be necessary to explain the spectrum of HgAr. We believe that the dissociation limit found from our study of the $3d \leftarrow 3p$ transitions in AlAr is correct, and that a similar double minimum (or at least a barrier to dissociation) is present in the $B\,{}^2\Sigma^+(4s)$ state of AlAr as well. Similar barriers may exist in the $B\,{}^2\Sigma^+(4s)$ state of AlKr, and in higher Rydberg states of both species, but the $B\,{}^2\Sigma^+(4s)$ state of AlAr is the only state for which we have strong evidence of such an effect.

C. Higher energy $nd \leftarrow 3p$ and $(n+1)s \leftarrow 3P$ excitations in AlAr and AlKr

1. The $5s \leftarrow 3p$ excitation in AlAr and AlKr

Figure 7 displays the $H\,{}^2\Sigma^+(5s) \leftarrow X_1\,{}^2\Pi_{1/2}(3p)$ band systems of AlAr and AlKr, as recorded using frequency-doubled coumarin 540A laser dye. Because the $3s^2 5s^1, {}^2S_{1/2}$ state of aluminum lies 1240 cm^{-1} away from any other excited electronic state, the spectra in this region are quite clean and only a single electronic state is observed. The preceding paper has presented a thorough analysis of the $H\,{}^2\Sigma^+(5s) \leftarrow X_1\,{}^2\Pi_{1/2}(3p)$ band system of AlKr,[16] so we will not comment upon it further here, except to state that

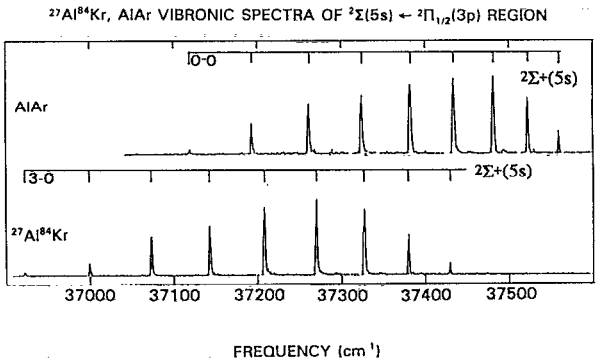

FIG. 7. The $H\,{}^2\Sigma^+(5s) \leftarrow X_1\,{}^2\Pi_{1/2}(3p)$ systems of AlAr (upper panel) and $^{27}Al\,{}^{84}Kr$ (lower panel), recorded using frequency-doubled coumarin 540A laser dye. In both molecules a simple vibrational progression with significant anharmonicity is observed.

our isotope shifts (measured in low resolution, but with mass spectrometric detection) are in full agreement with the assignment given there.

In the case of AlAr we are again troubled by the absence of isotopic information, which makes an absolute vibrational numbering difficult. By adopting the constraint that the bond strength of the various $^2\Sigma^+(ns)$ Rydberg states should monotonically increase with increasing n, however, and by experimenting with various numberings, the numbering given in Fig. 7 is found to be probably correct. Since this numbering assigns the first observed band as the 0–0 band, it gives a rigorous lower bound on the binding energy of the $H\,^2\Sigma^+(5s)$ state as $D_0[H\,^2\Sigma^+(5s), \mathrm{AlAr}] \geqslant 692\ \mathrm{cm}^{-1}$. Although, in principle, the numbering of the upper-state vibrational levels might be in error by as much as 2 quanta, the numbering given is most in accord with the other $^2\Sigma^+(ns) \leftarrow X_1\,^2\Pi_{1/2}(3p)$ band systems which are discussed below. As with the other band systems, band positions are available from the Physics Auxiliary Publication Service (PAPS) of the American Institute of Physics or from one of the authors (M.D.M.).[31]

2. The 4d←3p excitation in AlAr and AlKr

Figure 8 displays the spectra obtained in the range of 37 800–39 000 cm^{-1} for the $^2\Delta(4d) \leftarrow X_1\,^2\Pi_{1/2}(3p)$, $^2\Pi(4d) \leftarrow X_1\,^2\Pi_{1/2}(3p)$, and $^2\Sigma^+(4d) \leftarrow X_1\,^2\Pi_{1/2}(3p)$ systems of AlAr and AlKr. As was found for the $H\,^2\Sigma^+(5s)$ state, the $3s^2 4d\,^1,^2D$ state of aluminum is sufficiently far away from other electronic states that the spectra are relatively easy to interpret. Both molecules show three distinct vibrational progressions, which are identified in the figure. As in the $3d$ states, we assume that the term energies of the states fall in the order $^2\Delta(4d) < {}^2\Pi(4d) < {}^2\Sigma^+(4d)$, based on considerations of the ability of the $4d$ electron to shield the rare gas from the underlying Al^+ ion.

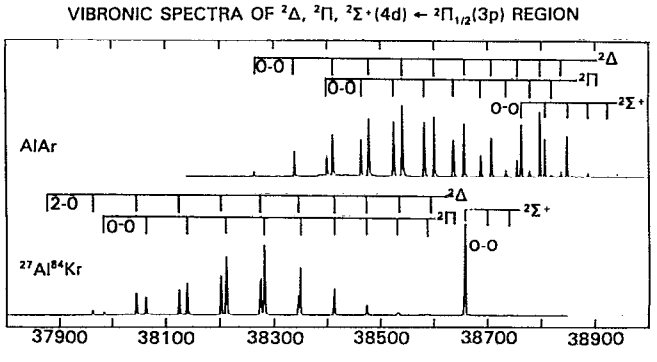

FIG. 8. The $^2\Delta(4d) \leftarrow X_1\,^2\Pi_{1/2}(3p)$, $^2\Pi(4d) \leftarrow X_1\,^2\Pi_{1/2}(3p)$, and $^2\Sigma^+(4d) \leftarrow X_1\,^2\Pi_{1/2}(3p)$ systems of AlAr (upper panel) and AlKr (lower panel), recorded using frequency-doubled coumarin 500 laser dye. In these spectra the three components are immediately evident, and assignment to the $^2\Delta(4d)$, $^2\Pi(4d)$, and $^2\Sigma^+(4d)$ states is straightforward, assuming that the states fall in the expected order of $^2\Delta < {}^2\Pi < {}^2\Sigma^+$.

In the spectrum of AlAr, the 0–0 bands of the $^2\Pi(4d) \leftarrow X_1\,^2\Pi_{1/2}(3p)$ and $^2\Sigma^+(4d) \leftarrow X_1\,^2\Pi_{1/2}(3p)$ systems are obvious, because they are relatively strong and no members of their respective progressions are found further to the red. The first band of the $^2\Delta(4d) \leftarrow X_1\,^2\Pi_{1/2}(3p)$ system, on the other hand, is rather weak, so a question remains as to the proper absolute vibrational numbering for this system. To maintain the rule that the bond strengths of successive $^2\Delta(nd)$ Rydberg states monotonically increase with increasing n, the first observed band must be assigned as either the 0–0 or 1–0 band, however. Moreover, in the higher-lying $^2\Delta(5d) \leftarrow X_1\,^2\Pi_{1/2}(3p)$, $^2\Delta(6d) \leftarrow X_1\,^2\Pi_{1/2}(3p)$, and $^2\Delta(7d) \leftarrow X_1\,^2\Pi_{1/2}(3p)$ band systems the 0–0 band is clearly observed, making it likely that the first observed band in the $^2\Delta(4d) \leftarrow X_1\,^2\Pi_{1/2}(3p)$ system is the 0–0 band as well. On this basis the assignments given in Fig. 8 were established.

In the case of AlKr the $^2\Sigma^+(4d) \leftarrow X_1\,^2\Pi_{1/2}(3p)$ band system is immediately evident as an intense 0–0 band followed at higher frequency by the very weak 1–0 and 2–0 bands. The distribution of intensity in this system implies that the bond length of the $^2\Sigma^+(4d)$ electronic state is nearly identical to that of the ground $^2\Pi_{1/2}(3p)$ state. The $^2\Delta(4d) \leftarrow X_1\,^2\Pi_{1/2}(3p)$ and $^2\Pi(4d) \leftarrow X_1\,^2\Pi_{1/2}(3p)$ band systems both show extended progressions with weak first bands, so the vibrational numbering is open to question. Isotope shifts have been measured in low resolution, however, and these help to clarify the assignment considerably. In the case of the $^2\Delta(4d) \leftarrow X_1\,^2\Pi_{1/2}(3p)$ system, the isotope shifts clearly show the first observed band to be the 2–0 band. In the $^2\Pi(4d) \leftarrow X_1\,^2\Pi_{1/2}(3p)$ system, on the other hand, the measured isotope shifts are less clear, and admit the possibility that the first observed band may be either the 0–0 or 1–0 band. We assign this first observed band as the 0–0 band, since this more easily preserves the rule that the bond strengths of the $^2\Pi(nd)$ Rydberg series should increase uniformly with increasing n.

3. The 6s←3p and 5d←3p excitations in AlAr and AlKr

The $3s^2 6s^1,^2S_{1/2}$ Rydberg level of atomic aluminum lies only about 91 cm^{-1} below the $3s^2 5d\,^1,^2D$ Rydberg level.[22] As a result, spectra of the $^2\Sigma^+(6s) \leftarrow X_1\,^2\Pi_{1/2}(3p)$, $^2\Delta(5d) \leftarrow X_1\,^2\Pi_{1/2}(3p)$, $^2\Pi(5d) \leftarrow X_1\,^2\Pi_{1/2}(3p)$, and $^2\Sigma^+(5d) \leftarrow X_1\,^2\Pi_{1/2}(3p)$ band systems may be expected to occur in the same energy range, as is evident in the spectra of AlAr and AlKr displayed in Fig. 9. Band positions are available from the Physics Auxiliary Publication Service (PAPS) of the American Institute of Physics or from one of the authors (M.D.M.).[31]

In examining the spectra of higher Rydberg states ($n \geqslant 5$) we have found the $^2\Sigma^+[(n+1)s] \leftarrow X_1\,^2\Pi_{1/2}(3p)$ band systems to be much weaker than the $^2\Delta(nd) \leftarrow X_1\,^2\Pi_{1/2}(3p)$ or $^2\Pi(nd) \leftarrow X_1\,^2\Pi_{1/2}(3p)$ systems, despite the fact that both occur in the same energy range. On the other hand, we have found that the $^2\Sigma^+[(n+1)s] \leftarrow X_1\,^2\Pi_{1/2}(3p)$ and $^2\Sigma^+(nd) \leftarrow X_1\,^2\Pi_{1/2}(3p)$ systems can be of similar intensity. Indeed, this behavior is sufficiently general that it can be used to differentiate the $^2\Delta(nd) \leftarrow X_1\,^2\Pi_{1/2}(3p)$ and $^2\Pi(nd) \leftarrow X_1\,^2\Pi_{1/2}(3p)$ sys-

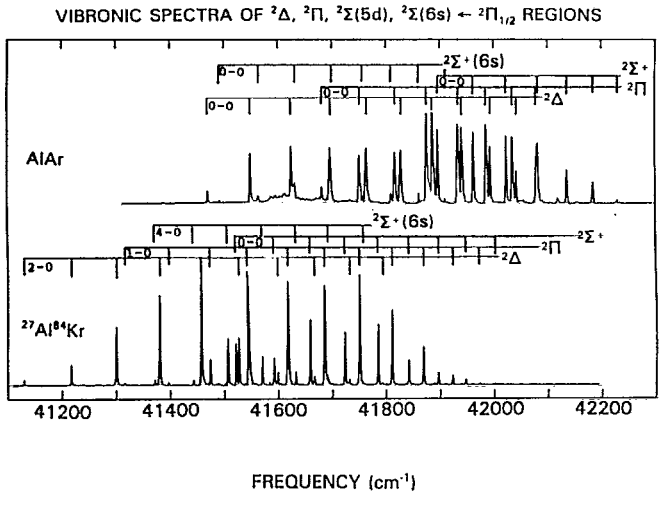

FIG. 9. The $^2\Delta(5d) \leftarrow X_1\,^2\Pi_{1/2}(3p)$, $^2\Pi(5d) \leftarrow X_1\,^2\Pi_{1/2}(3p)$, $^2\Sigma^+(5d) \leftarrow X_1\,^2\Pi_{1/2}(3p)$, and $^2\Sigma^+(6s) \leftarrow X_1\,^2\Pi_{1/2}(3p)$ systems of AlAr (upper panel) and AlKr (lower panel), recorded using frequency-doubled coumarin 480 laser dye. In these spectra the $5d \leftarrow 3p$ systems exhibit a much greater oscillator strength than does the $6s \leftarrow 3p$ system, allowing the spectra to be readily assigned. As discussed in the text, the weaker oscillator strength of the $6s \leftarrow 3p$ system is essentially an atomic property, which is preserved when the complex is formed.

tems from the $^2\Sigma^+[(n+1)s] \leftarrow X_1\,^2\Pi_{1/2}(3p)$ and $^2\Sigma^+(nd)$ tems from the $^2\Sigma^+[(n+1)s] \leftarrow X_1\,^2\Pi_{1/2}(3p)$ and $^2\Sigma^+(nd) \leftarrow X_1\,^2\Pi_{1/2}(3p)$ systems. Ultimately, this behavior can be traced to the atomic oscillator strengths, which have been critically evaluated by Wiese, Smith, and Miles.[34] These values show that the $3s^2nd\,^1,^2D \leftarrow 3s^23p^1,^2P^0$ transitions for $n \geqslant 5$ exhibit oscillator strengths which are at least a factor of 25 greater than the corresponding $3s^2(n+1)s$, $^2S \leftarrow 3s^23p,^2P^0$ transitions. This difference in oscillator strength is evidently carried over into the band systems of the complex, and greatly facilitates the assignment of features to the $(n+1)s \leftarrow 3p$ or $nd \leftarrow 3p$ systems. In some cases it is difficult to distinguish the $^2\Sigma^+(nd) \leftarrow X_1\,^2\Pi_{1/2}(3p)$ and $^2\Sigma^+[(n+1)s] \leftarrow X_1\,^2\Pi_{1/2}(3p)$ systems from one another, presumably because mixing of these two excited configurations leads to a partial equalization of oscillator strength between them.

The spectrum of AlAr in the $(6s,5d) \leftarrow 3p$ region shown in Fig. 9 displays three intense progressions. The $^2\Delta(5d) \leftarrow X_1\,^2\Pi_{1/2}(3p)$ system is expected to extend furthest to the red, since the bond strength of the $5d$ states is again expected to fall in the order $^2\Delta(5d) > {}^2\Pi(5d) > {}^2\Sigma^+(5d)$. Accordingly, the redmost system (beginning at 41 467 cm^{-1}) is assigned as the $^2\Delta(5d) \leftarrow X_1\,^2\Pi_{1/2}(3p)$ system. The next band system grows in intensity until it rivals the $^2\Delta(5d) \leftarrow X_1\,^2\Pi_{1/2}(3p)$ system near 41 750 cm^{-1}, and is assigned as the $^2\Pi(5d) \leftarrow X_1\,^2\Pi_{1/2}(3p)$ system. Finally, a third strong band system occurs with a strong origin band at 41 898 cm^{-1}. This is assigned as the $^2\Sigma^+(5d) \leftarrow X_1\,^2\Pi_{1/2}(3p)$ system. In the case of this $^2\Sigma^+(5d) \leftarrow X_1\,^2\Pi_{1/2}(3p)$ system the absolute vibrational numbering is obvious from the strong origin band. For the $^2\Delta(5d) \leftarrow X_1\,^2\Pi_{1/2}(3p)$ system, it must be assumed that the first observed band is the 0–0 band, since it is otherwise impossible to maintain the expectation that the bond strengths of the $^2\Delta(nd)$ states increase uniformly with increasing n. Finally, since the 0–0 bands are observed for both the $^2\Delta(5d) \leftarrow X_1\,^2\Pi_{1/2}(3p)$ and $^2\Sigma^+(5d) \leftarrow X_1\,^2\Pi_{1/2}(3p)$ systems, it seems reasonable that the first band observed in the $^2\Pi(5d) \leftarrow X_1\,^2\Pi_{1/2}(3p)$ system is also the 0–0 band, since the $^2\Pi(5d)$ state is assumed to lie between the $^2\Delta(5d)$ and $^2\Sigma^+(5d)$ states in bond strength (and presumably bond length).

In addition to these intense band systems, Fig. 9 shows a weak band system in the range of 41 489–41 910 cm^{-1}. This is by far the weakest of the band systems in this region, and must be assigned as the $^2\Sigma^+(6s) \leftarrow X_1\,^2\Pi_{1/2}(3p)$ system. The first observed band is again assigned as the 0–0 band, although in this case the vibrational numbering is less certain than in the $5d \leftarrow 3p$ band systems.

The analogous spectral region of AlKr also displays three relatively intense band systems and one weaker one. The assignment of the features to the $^2\Delta(5d) \leftarrow X_1\,^2\Pi_{1/2}(3p)$, $^2\Pi(5d) \leftarrow X_1\,^2\Pi_{1/2}(3p)$, $^2\Sigma^+(5d) \leftarrow X_1\,^2\Pi_{1/2}(3p)$, and $^2\Sigma^+(6s) \leftarrow X_1\,^2\Pi_{1/2}(3p)$ systems proceeds as in the case of AlAr, and is unambiguous. In the case of AlKr, however, we are again aided in the assignment of an absolute vibrational numbering by the measured isotope shifts. For the $^2\Sigma^+(5d) \leftarrow X_1\,^2\Pi_{1/2}(3p)$, $^2\Pi(5d) \leftarrow X_1\,^2\Pi_{1/2}(3p)$, and $^2\Sigma^+(6s) \leftarrow X_1\,^2\Pi_{1/2}(3p)$ systems the isotope shifts are rather definite in providing an absolute vibrational numbering. However, in the case of the $^2\Delta(5d) \leftarrow X_1\,^2\Pi_{1/2}(3p)$ system the assignment which gives the best fit (which identifies the first observed band as the 3–0 band) also gives a $^2\Delta(5d)$ state which is more strongly bound than the $AlKr^+$ ion. Since it is difficult to rationalize how this could occur, the first observed band of this system is assigned as the 2–0 band.

4. The $6d \leftarrow 3p$ and $7s \leftarrow 3p$ excitations in AlAr and AlKr

A situation very similar to that of the $(6s,5d) \leftarrow 3p$ excitations also occurs for the $(6d,7s) \leftarrow 3p$ excitations, since the $3s^26d\,^1,^2D$ level of Al lies only 105 cm^{-1} below the $3s^27s^1,^2S$ level. Accordingly, the band systems arising from these levels overlap one another (see Fig. 10), again making for a problematic assignment. In addition to this problem, the long-wavelength end of the spectrum of AlAr also contains transitions which we attribute to the $5f \leftarrow 3p$ excitation (see below), which becomes allowed in the complex because the orbitals distort somewhat from their shapes in the free atom.

In the spectrum of AlKr the $^2\Delta(6d) \leftarrow X_1\,^2\Pi_{1/2}(3p)$ and $^2\Pi(6d) \leftarrow X_1\,^2\Pi_{1/2}(3p)$ band systems are clearly visible as the two redmost and most intense progressions in this region. Although there is some scatter in the isotope shift measurements, the measured values are reasonably in accord with the values calculated for the assignment given. The assignment of the remaining features to the $^2\Sigma^+(6d) \leftarrow X_1\,^2\Pi_{1/2}(3p)$ and $^2\Sigma^+(7s) \leftarrow X_1\,^2\Pi_{1/2}(3p)$ systems is quite troublesome, however. Despite the large difference in oscillator strengths for the $6d \leftarrow 3p$ and $7s \leftarrow 3p$ atomic transitions,[34] these two systems exhibit similar intensity in the recorded spectrum (Fig. 10). This suggests that the $^2\Sigma^+(6d)$

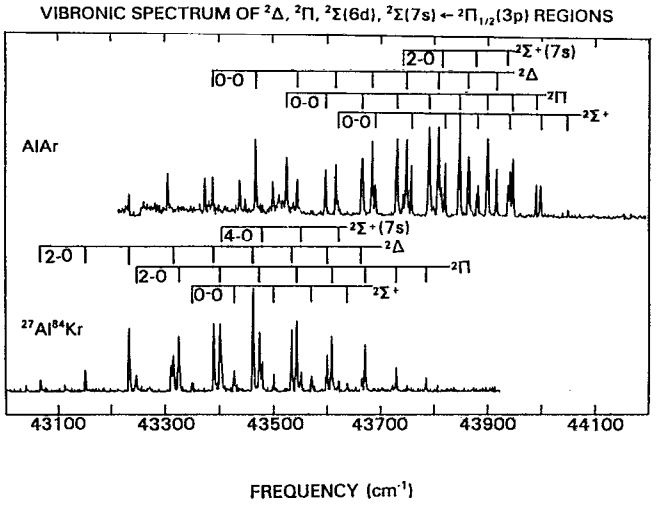

FIG. 10. The $^2\Delta(6d) \leftarrow X_1\,^2\Pi_{1/2}(3p)$, $^2\Pi(6d) \leftarrow X_1\,^2\Pi_{1/2}(3p)$, $^2\Sigma^+(6d) \leftarrow X_1\,^2\Pi_{1/2}(3p)$, and $^2\Sigma^+(7s) \leftarrow X_1\,^2\Pi_{1/2}(3p)$ systems of AlAr (upper panel) and AlKr (lower panel), recorded using frequency-doubled coumarin 460 laser dye. The assignment of the $^2\Delta(6d) \leftarrow X_1\,^2\Pi_{1/2}(3p)$ and $^2\Pi(6d) \leftarrow X_1\,^2\Pi_{1/2}(3p)$ systems is fairly straightforward, since they carry the large oscillator strength of the $6d \leftarrow 3p$ atomic transition. The assignment of the $^2\Sigma^+(6d) \leftarrow X_1\,^2\Pi_{1/2}(3p)$ and $^2\Sigma^+(7s) \leftarrow X_1\,^2\Pi_{1/2}(3p)$ systems is more problematic, however, as is described in the text. This may be due to configurational mixing of the two excited $^2\Sigma^+$ states, leading to a more nearly equal sharing of oscillator strength between them.

and $^2\Sigma^+(7s)$ states are strongly mixed, so that the intensity is equalized between them. In addition, the spectrum displayed in Fig. 10 was recorded with a damaged BBO crystal, leading to a poor signal-to-noise ratio; as a result the isotope shifts are far from definitive. Accordingly, neither the vibrational numbering nor the assignment as to which progression corresponds to the $^2\Sigma^+(6d) \leftarrow X_1\,^2\Pi_{1/2}(3p)$ or $^2\Sigma^+(7s) \leftarrow X_1\,^2\Pi_{1/2}(3p)$ system can be provided with confidence for AlKr.

In the case of AlAr the $^2\Delta(6d) \leftarrow X_1\,^2\Pi_{1/2}(3p)$ and $^2\Pi(6d) \leftarrow X_1\,^2\Pi_{1/2}(3p)$ band systems are likewise easily located as the most-intense band systems. In this case, however, the low energy end of the $(6d,7s) \leftarrow 3p$ spectral range shows additional features which cannot be assigned to any of the expected $^2\Delta(6d) \leftarrow X_1\,^2\Pi_{1/2}(3p)$, $^2\Pi(6d) \leftarrow X_1\,^2\Pi_{1/2}(3p)$, $^2\Sigma^+(6d) \leftarrow X_1\,^2\Pi_{1/2}(3p)$, or $^2\Sigma^+(7s) \leftarrow X_1\,^2\Pi_{1/2}(3p)$ band systems, and these also complicate the analysis. As is discussed in Sec. III D 2 below, these features are assigned to the forbidden $5f \leftarrow 3p$ atomic transition, which becomes weakly allowed when the aluminum atom is perturbed by a bound argon atom. Since the first observed member of the $^2\Pi(6d) \leftarrow X_1\,^2\Pi_{1/2}(3p)$ system possesses large intensity, it is assumed that it is the 0–0 band, leading to a definite assignment. The first observed band of the $^2\Delta(6d) \leftarrow X_1\,^2\Pi_{1/2}(3p)$ system is likewise assigned as the 0–0 band, since assigning it as the 1–0 band would give the $^2\Delta(6d)$ state a bond strength identical to that of the $AlAr^+$ ion, within 5 cm^{-1}. As in the case of AlKr discussed above, the remaining $^2\Sigma^+(6d)$ and $^2\Sigma^+(7s)$ states are somewhat difficult to distinguish, but we choose the more intense system as the $^2\Sigma^+(6d) \leftarrow X_1\,^2\Pi_{1/2}(3p)$ system, in accord with the greater oscillator strength of the $6d \leftarrow 3p$ transition as compared to the $7s \leftarrow 3p$ transition. If the 0–0 band is observed in both the $^2\Delta(6d) \leftarrow X_1\,^2\Pi_{1/2}(3p)$ and $^2\Pi(6d) \leftarrow X_1\,^2\Pi_{1/2}(3p)$ systems, it is expected that it would be observed in the $^2\Sigma^+(6d) \leftarrow X_1\,^2\Pi_{1/2}(3p)$ system as well, since the bond length of the ground state is expected to be more similar to the $^2\Sigma^+(6d)$ state than to either of the other two components of the $6d$ term. With this in mind the assignment given in Fig. 10 follows for the $6d \leftarrow 3p$ systems. On the other hand, the $^2\Sigma^+(7s) \leftarrow X_1\,^2\Pi_{1/2}(3p)$ system is rather weak, and if the first observed band were not the origin band, the preceding band would be buried under the 2–0 band of the $^2\Pi(6d) \leftarrow X_1\,^2\Pi_{1/2}(3p)$ system. In order to reach an assignment in which the bond strength of the $^2\Sigma^+(ns)$ series of states increases monotonically with n, the first observed band of the $^2\Sigma^+(7s) \leftarrow X_1\,^2\Pi_{1/2}(3p)$ system is assigned as the 2–0 band.

5. The $7d \leftarrow 3p$ excitation in AlAr

No assignable higher Rydberg states were observed in AlKr, primarily because the BBO doubling crystal required for these studies had been severely damaged. However, spectra of AlAr had been recorded prior to the catastrophe, so it is possible to continue with a description of the Rydberg states of this complex.

Figure 11 presents the spectrum of AlAr recorded in the region of the $7d \leftarrow 3p$ excitation (44 500–45 400 cm^{-1}). As in previous $nd \leftarrow 3p$ spectra, the $^2\Delta(7d) \leftarrow X_1\,^2\Pi_{1/2}(3p)$ and $^2\Pi(7d) \leftarrow X_1\,^2\Pi_{1/2}(3p)$ systems are the most intense and are the most easily assigned, provided one makes the assumption that the $^2\Delta(7d)$ state is more strongly bound than is the $^2\Pi(7d)$ state. As seems to be the case in most of the $nd \leftarrow 3p$ Rydberg series, the $^2\Sigma^+(7d) \leftarrow X_1\,^2\Pi_{1/2}(3p)$ system is more difficult to assign than are either the $^2\Delta(7d) \leftarrow X_1\,^2\Pi_{1/2}(3p)$ or $^2\Pi(7d) \leftarrow X_1\,^2\Pi_{1/2}(3p)$ systems. Two additional progressions have been located in Fig. 11 which may be candidates

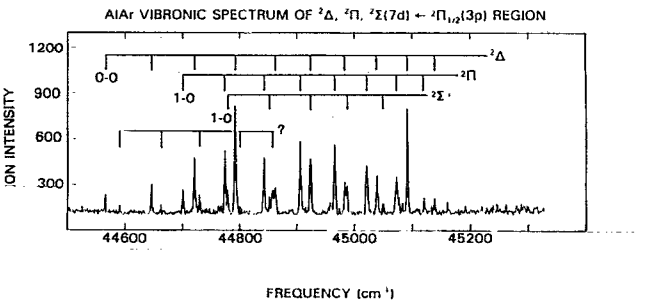

FIG. 11. The $^2\Delta(7d) \leftarrow X_1\,^2\Pi_{1/2}(3p)$, $^2\Pi(7d) \leftarrow X_1\,^2\Pi_{1/2}(3p)$, and $^2\Sigma^+(7d) \leftarrow X_1\,^2\Pi_{1/2}(3p)$ systems of AlAr, recorded using frequency-doubled coumarin 440 laser dye. The $^2\Delta(7d) \leftarrow X_1\,^2\Pi_{1/2}(3p)$ and $^2\Pi(7d) \leftarrow X_1\,^2\Pi_{1/2}(3p)$ systems are easily assigned on the basis of their intensity in the spectrum, but the $^2\Sigma^+(7d) \leftarrow X_1\,^2\Pi_{1/2}(3p)$ system is more problematic. See the text for details.

for the $^2\Sigma^+(7d) \leftarrow X_1\,^2\Pi_{1/2}(3p)$ system. The two progressions are of comparable intensity, but one is shifted too far to the red to be the $^2\Sigma^+(7d) \leftarrow X_1\,^2\Pi_{1/2}(3p)$ system. Accordingly, the remaining system is assigned as the $^2\Sigma^+(7d) \leftarrow X_1\,^2\Pi_{1/2}(3p)$ system. Band positions for all of the $7d \leftarrow 3p$ systems are available from the Physics Auxiliary Publication Service (PAPS) of the American Institute of Physics or from one of the authors (M.D.M.),[31] along with corresponding band positions for the $8d \leftarrow 3p$ and $9d \leftarrow 3p$ systems.

The remaining band system which has been identified in Fig. 11 extends too far to the red to be the expected $^2\Sigma^+(8s) \leftarrow X_1\,^2\Pi_{1/2}(3p)$ system. At this point it remains unidentified, although it is likely that it may be one of the components of the $6f \leftarrow 3p$ transition, which may gain intensity by mixing of the $6f$ and $7d$ orbitals in the presence of the perturbing argon atom.

6. The $8d \leftarrow 3p$ excitation in AlAr

In contrast to the $7d \leftarrow 3p$ band systems, the spectrum of the $8d \leftarrow 3p$ transition in AlAr is very clean, with all three components clearly evident. This is illustrated in Fig. 12, which displays the 45 300–45 900 spectral region in which this set of bands occurs. The $^2\Delta(8d) \leftarrow X_1\,^2\Pi_{1/2}(3p)$ and $^2\Pi(8d) \leftarrow X_1\,^2\Pi_{1/2}(3p)$ bands occur in pairs, with a separation of only 10–15 cm^{-1}. This indicates that the $^2\Delta(8d)$ and $^2\Pi(8d)$ potentials are becoming very similar indeed, and an approach to Hund's case (d) is taking place. At higher frequencies the $^2\Sigma^+(8d) \leftarrow X_1\,^2\Pi_{1/2}(3p)$ system becomes evident, displaying only slightly less intensity than the $^2\Delta(8d) \leftarrow X_1\,^2\Pi_{1/2}(3p)$ and $^2\Pi(8d) \leftarrow X_1\,^2\Pi_{1/2}(3p)$ systems. Again, band positions are available for all three systems through the Physics Auxiliary Publication Service (PAPS) of the American Institute of Physics or from one of the authors (M.D.M.).[31]

7. The $9d \leftarrow 3p$ excitation in AlAr

Assignment of the $9d \leftarrow 3p$ band system (and higher Rydberg states) becomes extremely problematic, since band systems belonging to various $nd \leftarrow 3p$ transitions begin to overlap above $n \approx 9$. Thus, although discrete transitions continue to be observable for another 1550 cm^{-1} above the 0–0 bands of the $9d \leftarrow 3p$ systems, no definite assignment is yet possible for these systems. To be definite it would be very desirable to investigate the systems with much higher resolution, so that electronic symmetry species could be assigned without doubt. In addition, a suitable optical–optical double-resonance experiment, taking advantage of the similarity between vibrational wave functions in the various high Rydberg states, could certainly simplify the assignment.

In any case, Fig. 13 displays the 45 800–46 400 cm^{-1} spectral range in which the $9d \leftarrow 3p$ band systems are expected. As is obvious from the figure, more transitions are present than can be explained on the basis of the $9d \leftarrow 3p$ systems alone. However, the most intense systems in this range may be interpreted as the $^2\Delta(9d) \leftarrow X_1\,^2\Pi_{1/2}(3p)$, $^2\Pi(9d) \leftarrow X_1\,^2\Pi_{1/2}(3p)$, and $^2\Sigma^+(9d) \leftarrow X_1\,^2\Pi_{1/2}(3p)$ systems, as are indicated in the figure. Toward higher frequencies bands that are certainly due to the $10d \leftarrow 3p$ system begin to intrude; we have not been successful in obtaining a definite assignment of these bands, however, and they will not be discussed further. In addition, another band system [tentatively identified as the $^2\Sigma^+(10s) \leftarrow X_1\,^2\Pi_{1/2}(3p)$ system] is indicated in Fig. 13, and band positions are available through the Physics Auxiliary Publication Service (PAPS) of the American Institute of Physics or from one of the authors (M.D.M.).[31]

D. Electric dipole forbidden transitions, made allowed in the complex

1. The $4f \leftarrow 3p$ excitation in AlAr and AlKr

The $4f \leftarrow 3p$ spectra of AlAr and AlKr provide the clearest example of an electric dipole forbidden transition in atomic aluminum which becomes weakly allowed when aluminum is complexed with a rare gas. The $3s^2 4f\,^1,^2F^0$ levels of

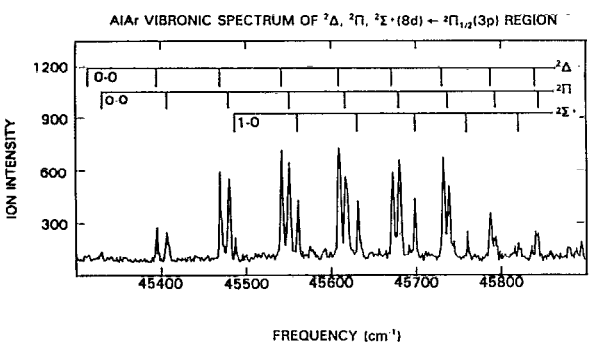

FIG. 12. The $^2\Delta(8d) \leftarrow X_1\,^2\Pi_{1/2}(3p)$, $^2\Pi(8d) \leftarrow X_1\,^2\Pi_{1/2}(3p)$, and $^2\Sigma^+(8d) \leftarrow X_1\,^2\Pi_{1/2}(3p)$ systems of AlAr, recorded using frequency-doubled coumarin 440 laser dye. In this spectral region the three components of the $3s^2 8d\,^1,^2D$ state are readily observed, with little difficulty in assignment.

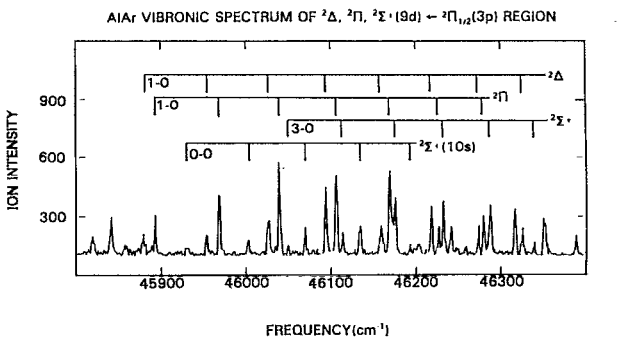

FIG. 13. The $^2\Delta(9d) \leftarrow X_1\,^2\Pi_{1/2}(3p)$, $^2\Pi(9d) \leftarrow X_1\,^2\Pi_{1/2}(3p)$, and $^2\Sigma^+(9d) \leftarrow X_1\,^2\Pi_{1/2}(3p)$ systems of AlAr, recorded using frequency-doubled stilbene 420 laser dye. In this spectral range and higher, band systems associated with different principal quantum numbers begin to overlap, making assignment difficult. The labeled systems provide our best guess as to the $^2\Delta(9d) \leftarrow X_1\,^2\Pi_{1/2}(3p)$, $^2\Pi(9d) \leftarrow X_1\,^2\Pi_{1/2}(3p)$, $^2\Sigma^+(9d) \leftarrow X_1\,^2\Pi_{1/2}(3p)$, and $^2\Sigma^+(10s) \leftarrow X_1\,^2\Pi_{1/2}(3p)$ systems.

aluminum lie 1041 cm^{-1} above the $3s^25p^1,^2P^0_{3/2}$ level and 826.1 cm^{-1} below the $3s^26s^1,^2S_{1/2}$ level, substantially isolating them from other electronic states. Accordingly, the $4f \leftarrow 3p$ transitions in the AlAr and AlKr complexes are expected to be rather isolated in the spectrum, and are expected approximately 830 cm^{-1} lower in frequency than the $^2\Sigma^+(6s) \leftarrow X_1\,^2\Pi_{1/2}(3p)$ band system. Thus one is led to search for the $4f \leftarrow 3p$ transitions in the range of 40 660–41 080 cm^{-1} for AlAr and 40 200–40 860 cm^{-1} for AlKr.

Figure 14 demonstrates that transitions are indeed found in the expected spectral regions in our studies of AlAr and AlKr. An interesting point is that the bands associated with these transitions are more easily observed at the mass of aluminum atomic ions ($m/e = 27$), rather than at the mass of AlAr ($m/e = 67$) or AlKr ($m/e = 109$–113). Excitation of the $4f$ states apparently leads to an efficient fragmentation process. As is discussed in Sec. III E below, this photofragmentation process is almost certainly occurring by rapid predissociation of the $4f$ state of the complex, followed by photoionization of an electronically excited aluminum atom.

Although one might imagine that the $4f \leftarrow 3p$ bands observed in Fig. 14 could arise as electric dipole allowed two-photon transitions resulting from the fundamental dye laser radiation (which is admitted into the ionization region along with the second-harmonic, ultraviolet radiation), this cannot be the case, because one would then expect to observe the $3s^24f^1,^2F^0 \overset{2h\nu}{\leftarrow} 3s^23p^1,\,^2P^0$ transitions of atomic aluminum at 41 318.74 and 41 206.70 cm^{-1} as well. Moreover, these atomic transitions would be expected to be *more* intense than the transitions of the complex, since many more aluminum atoms are present in the molecular beam, and the atoms would not spread their oscillator strength over several vibrational transitions.

With this fact in mind, the observation of bands corresponding to the electric dipole forbidden, $3s^24f^1,^2F^0 \leftarrow 3s^23p^1,^2P^0$, transition of atomic aluminum must imply that the $3p$ (and/or $4f$) orbitals of aluminum are distorted from their atomic shapes by the presence of a rare-gas ligand. One can easily imagine that the $3p\pi$ orbital, which is singly occupied in the ground state of the complex, could reduce its orbital energy by mixing with the $3d\pi$ orbital, allowing it to polarize away from the rare gas. A small component of $3d\pi$ character in the ground-state wave function would then allow transitions which are nominally $4f\delta \leftarrow 3p\pi$, $4f\pi \leftarrow 3p\pi$, and $4f\sigma \leftarrow 3p\pi$ in character to gain intensity. Of course, contamination of the $4f\sigma$, $4f\pi$, and $4f\delta$ orbitals with $3d\sigma$, $3d\pi$, and $3d\delta$ character, respectively, would likewise allow the $4f$ orbitals to become polarized and would make the $4f \leftarrow 3p$ transitions weakly allowed. In either case it is the destruction of the center of inversion of the atom which causes the transition to possess a nonvanishing intensity. A measurement of the absolute intensity of the $3d \leftarrow 3p$ and $4f \leftarrow 3p$ absorption bands would allow an estimate of the $3d$ character of the $3p\pi$, $4f\delta$, $4f\pi$, and $4f\sigma$ orbitals to be made, and would provide a very interesting comparison with theory. This is difficult in the present experiments, however, because of the intrinsic nonlinearity of the two-photon ionization process and the unknown quantum yields for production of ionizable states of the fragment aluminum atom.

2. The 5f ← 3p and 6p ← 3p excitations in AlAr

A similar situation is encountered in the $5f \leftarrow 3p$ and $6p \leftarrow 3p$ excitations of AlAr, except that the spectra fall in a more congested region, making assignments more difficult. Nevertheless, Fig. 15 displays the spectra of the $5f \leftarrow 3p$ and $6p \leftarrow 3p$ transitions of AlAr, and band positions are available through the Physics Auxiliary Publication Service (PAPS) of the American Institute of Physics or from one of the au-

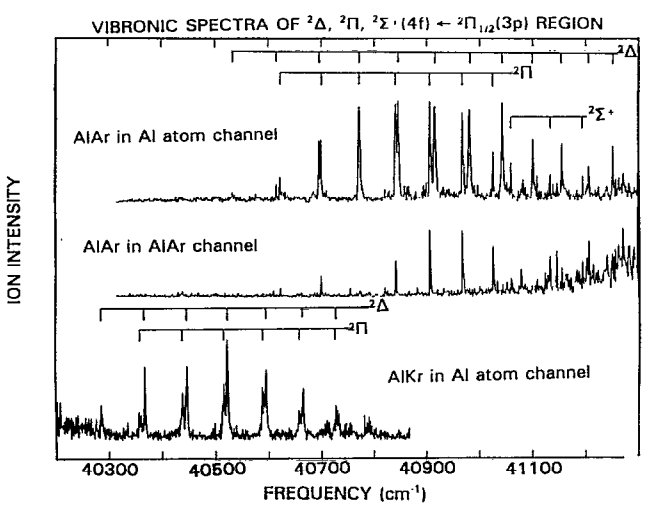

FIG. 14. The $^2\Delta(4f) \leftarrow X_1\,^2\Pi_{1/2}(3p)$, $^2\Pi(4f) \leftarrow X_1\,^2\Pi_{1/2}(3p)$, and $^2\Sigma^+(4f) \leftarrow X_1\,^2\Pi_{1/2}(3p)$ systems of AlAr (upper panels) and AlKr (lowest panel), recorded using frequency-doubled coumarin 500 and 480 laser dyes. These transitions show up prominently at the aluminum atomic mass, indicating rapid predissociation of the excited electronic state to form ionizable excited-state aluminum atoms. The observation of any of these electric dipole forbidden systems implies a distortion of the orbitals from their shapes in the isolated atom.

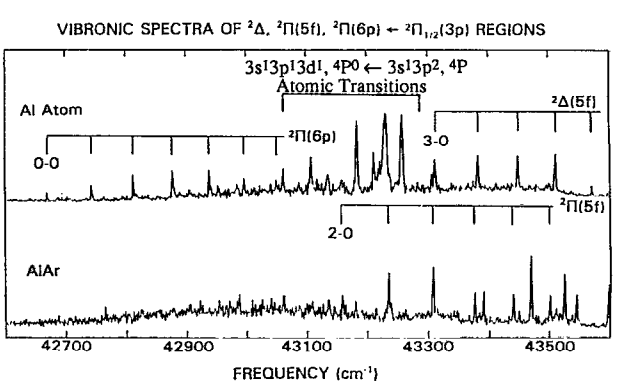

FIG. 15. The $^2\Delta(5f) \leftarrow X_1\,^2\Pi_{1/2}(3p)$, $^2\Pi(5f) \leftarrow X_1\,^2\Pi_{1/2}(3p)$, and $^2\Pi(6p) \leftarrow X_1\,^2\Pi_{1/2}(3p)$ systems of AlAr, as observed at the mass of aluminum (upper panel) and AlAr (lower panel). The atomic transitions in the range 43 060–43 260 cm^{-1} originate from metastable $3s^13p^2,^4P$ aluminum atoms and unfortunately interfere with the assignment of the origin bands of the $^2\Delta(5f) \leftarrow X_1\,^2\Pi_{1/2}(3p)$ and $^2\Pi(5f) \leftarrow X_1\,^2\Pi_{1/2}(3p)$ systems.

thors (M.D.M.).[31] Again, these electric dipole forbidden transitions are more prominent in the spectra collected at the mass of the aluminum atom than at the mass of AlAr. This is unfortunate, since a number of atomic transitions (primarily the $3s^1 3p^1 3d^1$, $^4P^0_{J'} \leftarrow 3s^1 3p^2, ^4P_{J''}$ transitions, arising from metastable $3s^1 3p^2, ^4P_{J''}$ atoms) obscure the features of the complex in the range 43 061–43 257 cm^{-1}. This is the region in which the 0–0 bands of the $^2\Delta(5f) \leftarrow X_1\,^2\Pi_{1/2}(3p)$ and $^2\Pi(5f) \leftarrow X_1\,^2\Pi_{1/2}(3p)$ systems are expected, and may also correspond the region in which the $^2\Sigma^+(6p) \leftarrow X_1\,^2\Pi_{1/2}(3p)$ band system occurs as well.

E. State-dependent fragmentation behavior

As noted above, many band systems are observed in the mass channels of both the complex and the aluminum atomic ion. In some cases (such as the $3d \leftarrow 3p$ and $4d \leftarrow 3p$ systems of AlAr and AlKr) very little signal is observed at the atomic mass. In other cases (such as the $4f \leftarrow 3p$ band systems of AlAr and AlKr, and the $6p \leftarrow 3p$ band systems of AlAr), the band systems would have gone undetected if the atomic mass channel had not been monitored. There also exist cases in which the fragmentation yield increases substantially with increasing v' in a band system (as in the $5s \leftarrow 3p$ system of AlKr), or in which one component of a system is strongly dissociated while others are unaffected [as occurs in the $^2\Delta(5d)$ state of AlKr, which dissociates in high yield above $v' = 5$, while the $^2\Pi(5d)$ and $^2\Sigma^+(5d)$ states are relatively unaffected, as displayed in Fig. 16].

These observations strongly suggest that the mechanism of dissociation consists of absorption of a photon to produce the excited state of the complex, followed by rapid predissociation (within 5 ns) leading to a ground-state rare-gas atom and an *electronically excited* aluminum atom. Finally, the electronically excited aluminum atom is ionized by absorption of a second photon, resulting in the observation of a band spectrum at the mass of aluminum. Alternative processes in which the excited state of the complex is ionized by absorption of a second photon, and the resulting $AlAr^+$ or $AlKr^+$ ion subsequently dissociates, cannot readily explain the state selectivity of the dissociation process. An important factor in reaching this conclusion is that the ground state of the aluminum cation is $3s^2, ^1S_0$, and the first excited state is $3s^1 3p^1, ^3P^0_0$, lying 37 392.0 cm^{-1} above the cationic ground state.[22] This lies so high in energy that it is inaccessible in our presumed two-photon experiments. In addition, it could not be reached in a three-photon process in which a third photon is absorbed by the $^1\Sigma^+$ ground state of the $AlAr^+$ or $AlKr^+$ ion, because of spin selection rules. Furthermore, the first excited singlet state of Al^+ ($3s^1 3p^1, ^1P^0$) lies 59 849.7 cm^{-1} above the $^1S_0$ ground state,[22] far beyond the accessible range of the present experiments. Accordingly, the only dissociation mechanism that could occur *following* ionization of a bound complex is direct excitation to the vibrational continuum of the $X\,^1\Sigma^+$ state of the $AlAr^+$ or $AlKr^+$ cation. Although this could certainly occur, and the process could even be favored if the potential curves of the ion and the excited state of the complex were very different, there is no reason to expect such dramatic differences in potential curves when comparing Rydberg states of the neutral with the ground state of the ion.

With these factors in mind, it appears that the excited states of AlAr and AlKr suffer predissociation through couplings with lower excited electronic states. Thus, for example, the $H\,^2\Sigma^+(5s)$ state of AlKr probably predissociates by nonadiabatic coupling with the $^2\Sigma^+(3d)$ state which is only weakly bound, and lies some 5000 cm^{-1} lower in energy. Indeed, high-resolution spectra of the $H\,^2\Sigma^+(5s) \leftarrow X_1\,^2\Pi_{1/2}(3p)$ system have been used to construct an RKR potential curve for the $H\,^2\Sigma^+(5s)$ state,[16] and it has been suggested that this potential has been modified by an avoided curve crossing with the $^2\Sigma^+(3d)$ state.[16] Such an avoided crossing could readily lead to predissociation induced by nonadiabatic coupling of the two adiabatic states. A compelling test of this hypothesis would be to determine if aluminum atoms are produced in the $3s^2 3d, ^2D$ state following excitation of the $H\,^2\Sigma^+(5s) \leftarrow X_1\,^2\Pi_{1/2}(3p)$ band system. Similar probes of the electronic state distributions of the aluminum atomic fragments would be very helpful in untangling the complicated dissociation dynamics of higher Rydberg states as well.

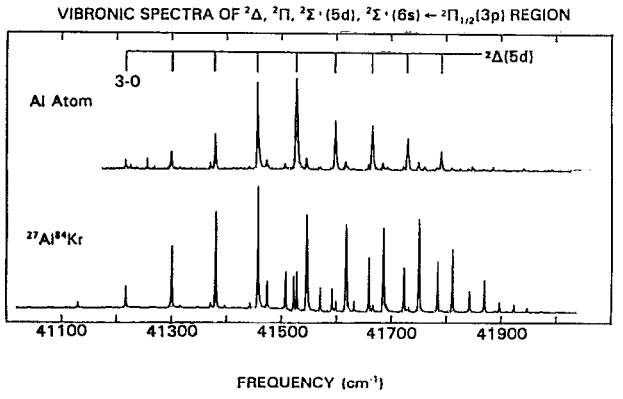

FIG. 16. Spectra of the $^2\Delta(5d) \leftarrow X_1\,^2\Pi_{1/2}(3p)$, $^2\Pi(5d) \leftarrow X_1\,^2\Pi_{1/2}(3p)$, $^2\Sigma^+(5d) \leftarrow X_1\,^2\Pi_{1/2}(3p)$, and $^2\Sigma^+(6s) \leftarrow X_1\,^2\Pi_{1/2}(3p)$ systems of AlKr, as observed at the mass of $^{27}Al\,^{84}Kr$ (lower panel) and ^{27}Al (upper panel). Here it is evident that predissociation of the $^2\Delta(5d)$ state occurs far more readily than does predissociation of the other states in this region.

IV. DISCUSSION

A. Bonding trends and comparisons between AlAr and AlKr

Tables I and II present a summary of the electronic states of AlAr and AlKr, as deduced from this work and the work of previous investigators. Since the monotone increasing character of the bond strength as a function of principal quantum number n was used to make vibrational assignments, it is not surprising that this behavior is found. Of greater interest is the fact that the fundamental vibrational frequency ω_e undergoes a nearly monotonic increase with principal quantum number in the $^2\Delta(nd)$ and $^2\Pi(nd)$ series. This monotonic behavior is observed in the $^2\Delta(nf)$, $^2\Pi(nf)$,

TABLE I. Electronic states of $^{27}Al\,^{40}Ar$. Throughout this table error estimates are provided in parentheses following each entry, representing the 1σ error limits in units of the last digit quoted for the corresponding measured quantity. Thus, for example, $D_0(X_1\,^2\Pi_{1/2}) = 122.4 \pm 4.0\ cm^{-1}$.

State	T_0 (cm^{-1})	ω_e (cm^{-1})	$\omega_e x_e$ (cm^{-1})	D_0 (cm^{-1})	Δ	Δ(Al)	Δ(Al)–Δ	Vibrational numbering	Electronic assignment
$^2\Sigma^+(10s)$	45 930.46(37)	75.95(54)	2.08(11)	857.6	1.412	1.751	0.339	$\Delta v' = +1$ possible	Tentative
$^2\Sigma^+(7s)$	43 577.93(160)	92.44(112)	3.43(14)	817.6	1.655	1.766	0.111	$\Delta v' = +1$ possible but unlikely	Fairly definite, based on oscillator strength
$^2\Sigma^+(6s)$	41 489.22(37)	75.87(35)	1.98(4)	778.0	1.698	1.770	0.072	$\Delta v' = +1$ possible but unlikely	Definite, based on oscillator strength
$H\,^2\Sigma^+(5s)$	37 119.66(23)	78.82(15)	2.65(2)	692.1	1.736	1.781	0.045	$\Delta v' = +1$ possible but unlikely	Definite (isolated band system)
$B\,^2\Sigma^+(4s)$[a]	25 113.4	84.50(155)[b]	4.88(78)[b]	356.7	1.782	1.812	0.030	Certain (RKR gives good *FC* factor)	Definite (isolated band system)
$^2\Pi(6p)$	42 669.55(22)	76.83(19)	1.92(3)	787.8	1.193	1.288	0.095	$\Delta v' = +1, +2$ possible (unlikely)	Could be $^2\Sigma^+(6p)$, but unlikely
$^2\Pi(4p)$(?)	32 328.16(32)	66.64(68)	1.64(17)	744.1	1.303	1.324	0.021	Tentative at best	Tentative at best
$X_1\,^2\Pi_{1/2}(3p)$[c]	0.00	31.60(203)[d]	1.51(70)[d]	122.4(40)	1.479	1.492	0.013	Definite (ground state)	Definite (ground state)
$^2\Delta(9d)$	45 798.64(95)	83.87(54)	2.01(5)	917.0	0.769	0.930	0.161		Likely, assuming $^2\Delta(9d) < ^2\Pi(9d) < ^2\Sigma^+(9d)$
$^2\Delta(8d)$	45 314.79(45)	83.34(29)	1.98(3)	901.5	0.778	0.912	0.134	Definite, assuming D_0	Definite, assuming $^2\Delta(8d) < ^2\Pi(8d) < ^2\Sigma^+(8d)$
$^2\Delta(7d)$	44 564.93(74)	83.86(42)	2.01(4)	901.6	0.799	0.885	0.086	increases with increasing n.	Definite, assuming $^2\Delta(7d) < ^2\Pi(7d) < ^2\Sigma^+(7d)$
$^2\Delta(6d)$	43 389.48(21)	83.45(14)	1.96(2)	899.4	0.781	0.834	0.053		Definite, assuming $^2\Delta(6d) < ^2\Pi(6d) < ^2\Sigma^+(6d)$
$^2\Delta(5d)$	41 466.49(69)	84.72(39)	2.10(4)	889.6	0.706	0.739	0.033		Definite, assuming $^2\Delta(5d) < ^2\Pi(5d) < ^2\Sigma^+(5d)$
$^2\Delta(4d)$	38 264.47(23)	79.32(12)	2.00(1)	787.4	0.538	0.574	0.036	$\Delta v' = +1$ possible but unlikely	Definite, assuming $^2\Delta(4d) < ^2\Pi(4d) < ^2\Sigma^+(4d)$
$^2\Delta(3d)$	32 032.83(26)	66.12(20)	1.99(2)	525.0	0.329	0.368	0.039	$\Delta v' = +1, +2$ possible but unlikely	Definite, assuming $^2\Delta(3d) < ^2\Pi(3d) < ^2\Sigma^+(3d)$
$^2\Pi(9d)$	45 813.90(83)	83.88(53)	2.17(6)	901.8	0.730	0.930	0.200	Definite, assuming D_0	Likely, assuming $^2\Delta(9d) < ^2\Pi(9d) < ^2\Sigma^+(9d)$
$^2\Pi(8d)$	45 329.44(49)	81.45(32)	1.91(3)	886.9	0.752	0.912	0.160	increases with increasing n.	Definite, assuming $^2\Delta(8d) < ^2\Pi(8d) < ^2\Sigma^+(8d)$
$^2\Pi(7d)$	44 623.91(52)	81.05(30)	2.12(3)	842.7	0.734	0.885	0.151		Definite, assuming $^2\Delta(7d) < ^2\Pi(7d) < ^2\Sigma^+(7d)$
$^2\Pi(6d)$	43 524.34(29)	77.01(19)	2.09(2)	764.5	0.691	0.834	0.143	Definite (strong 0–0 band)	Definite, assuming $^2\Delta(6d) < ^2\Pi(6d) < ^2\Sigma^+(6d)$
$^2\Pi(5d)$	41 680.32(106)	74.27(80)	2.20(10)	675.8	0.627	0.739	0.112	$\Delta v' = +1$ possible but unlikely	Definite, assuming $^2\Delta(5d) < ^2\Pi(5d) < ^2\Sigma^+(5d)$
$^2\Pi(4d)$	38 399.52(17)	67.98(11)	1.73(1)	652.3	0.512	0.574	0.062	Definite (strong 0–0 band)	Definite, assuming $^2\Delta(4d) < ^2\Pi(4d) < ^2\Sigma^+(4d)$
$^2\Pi(3d)$	32 421.22(80)	21.64(72)	1.15(10)	136.6	0.295	0.368	0.073	Definite (strong 0–0 band)	Definite, assuming $^2\Delta(3d) < ^2\Pi(3d) < ^2\Sigma^+(3d)$
$^2\Sigma^+(9d)$	45 839.21(258)	76.23(109)	1.53(9)	876.5	0.664	0.930	0.266	$\Delta v' = +1$ possible but unlikely	Likely, assuming $^2\Delta(9d) < ^2\Pi(9d) < ^2\Sigma^+(9d)$
$^2\Sigma^+(8d)$	45 409.40(81)	81.28(61)	1.85(7)	806.9	0.610	0.912	0.302	$\Delta v' = +1$ possible but unlikely	Definite, assuming $^2\Delta(8d) < ^2\Pi(8d) < ^2\Sigma^+(8d)$
$^2\Sigma^+(7d)$	44 701.08(52)	81.06(51)	1.90(7)	765.5	0.645	0.885	0.240	If $^2\Sigma^+(8s)$, $\Delta v' = -1$ likely	Weak band system, probably $^2\Sigma^+(7d)$, possibly $^2\Sigma^+(8s)$
$^2\Sigma^+(6d)$	43 620.68(55)	72.21(41)	1.36(5)	668.2	0.625	0.834	0.209	$\Delta v' = +1$ possible but unlikely	Definite, based on oscillator strength
$^2\Sigma^+(5d)$	41 896.49(114)	68.83(103)	1.89(14)	459.6	0.542	0.739	0.197	Definite (strong 0–0 band)	Definite, assuming $^2\Delta(5d) < ^2\Pi(5d) < ^2\Sigma^+(5d)$
$^2\Sigma^+(4d)$	38 763.12(14)	46.45(20)	1.27(4)	288.7	0.439	0.574	0.135	Definite (strong 0–0 band)	Definite, assuming $^2\Delta(4d) < ^2\Pi(4d) < ^2\Sigma^+(4d)$
$^2\Sigma^+(3d)$(?)	32 517.53(23)	8.87(26)	0.27(4)	40.3	0.286	0.368	0.082	Tentative at best	Tentative at best
$^2\Delta(5f)$	42 992.92(118)	88.35(63)	1.98(6)	960.6	0.020	0.033	0.013	Definite, assuming D_0 increases with n	Definitely $5f$, probably $^2\Delta(5f)$
$^2\Delta(4f)$	40 533.82(51)	87.48(23)	1.85(2)	907.3	0.008	0.029	0.021	Definite, assuming $D_0 < D_0$ (ion)	Definitely $4f$, probably $^2\Delta(4f)$
$^2\Pi(5f)$	43 071.45(79)	89.22(41)	2.28(4)	882.0	−0.024	0.033	0.057	$\Delta v' = +1$ possible but unlikely	Definitely $5f$, probably $^2\Pi(5f)$
$^2\Pi(4f)$	40 624.13(15)	80.28(13)	1.91(2)	817.0	−0.019	0.029	0.048	$\Delta v' = +1$ possible but unlikely	Definitely $4f$, probably $^2\Pi(4f)$
$^2\Sigma^+(4f)$	41 059.29	84.72	5.72	381.9	−0.154	0.029	0.183	$\Delta v' = +1 - +4$ possible	Weak transitions, probably $^2\Sigma^+(4f)$
$^1\Sigma^+$(ion)	47 418.5(20)			982.3(50)					

[a] Rotational constants for $B\,^2\Sigma^+(4s)$ from Ref. 15: $B_e = 0.112\,42(11)$; $\alpha_e = 0.001\,10(2)$; $\gamma_e = 0.000\,52(5)$; $r_e = 3.05(1)$ Å.

[b] From Ref. 15

[c] Rotational constants for $X_1\,^2\Pi_{1/2}(3p)$ from Ref. 15: $B_e = 0.0727(5)$; $\alpha_e = 0.0036(5)$; $r_e = 3.79(1)$ Å.

[d] From Ref. 13.

TABLE II. Electronic states of $^{27}Al\,^{84}Kr$[a].

State	T_0 (cm^{-1})	ω_e (cm^{-1})	$\omega_e x_e$ (cm^{-1})	D_0 (cm^{-1})	Δ	Δ(Al)	Δ(Al)−Δ	Vibrational numbering	Electronic assignment
$^2\Sigma^+(7s)$	43 084.16(852)	85.84(348)	1.13(29)	1383.7	1.671	1.766	0.095	Tenuous at best	Could be $^2\Sigma^+(6d)$ or a mixed $^2\Sigma^+(6d$–$7s)$ state
$^2\Sigma^+(6s)$	41 070.79(742)	81.93(257)	1.31(18)	1268.8	1.679	1.770	0.091	Definite (isotope shifts)	Definite, based on oscillator strength
$H\,^2\Sigma^+(5s)$[b]	36 668.25(10)	93.44(4)	2.01(1)	1215.8	1.733	1.781	0.048	Definite (Ref. 16)	Definite (isolated band system)
$B\,^2\Sigma^+(4s)$[c]	24 581.69(37)	99.16(21)	1.75(3)	960.7	1.785	1.812	0.027	Definite (Ref. 16)	Definite (isolated band system)
$X_1\,^2\Pi_{1/2}(3p)$[d]	0.00	39.0(282)[e]	1.93(70)[e]	194.7(8)	1.471	1.492	0.021	Definite (ground state)	Definite (ground state)
$^2\Delta(6d)$	42 887.27(141)	94.72(57)	1.55(4)	1473.9	0.802	0.834	0.032	Nearly definite (isotope shifts)	Definite, assuming $^2\Delta(6d) < {}^2\Pi(6d) < {}^2\Sigma^+(6d)$
$^2\Delta(5d)$	40 949.03(202)	95.75(81)	1.60(6)	1479.4	0.723	0.739	0.016	$\Delta v' = +1$ possible but unlikely	Definite, assuming $^2\Delta(5d) < {}^2\Pi(5d) < {}^2\Sigma^+(5d)$
$^2\Delta(4d)$	37 695.17(39)	95.60(14)	1.61(1)	1429.0	0.556	0.574	0.018	Definite (isotope shifts)	Definite, assuming $^2\Delta(4d) < {}^2\Pi(4d) < {}^2\Sigma^+(4d)$
$^2\Delta(3d)$	31 498.23(45)	86.28(15)	1.62(1)	1131.9	0.335	0.368	0.033	Definite (isotope shifts)	Definite, assuming $^2\Delta(3d) < {}^2\Pi(3d) < {}^2\Sigma^+(3d)$
$^2\Pi(6d)$	43 078.83(70)	89.30(28)	1.70(2)	1282.4	0.675	0.834	0.159	Nearly definite (isotope shifts)	Definite, assuming $^2\Delta(6d) < {}^2\Pi(6d) < {}^2\Sigma^+(6d)$
$^2\Pi(5d)$	41 232.54(79)	86.68(33)	1.60(2)	1195.9	0.619	0.739	0.120	Definite (isotope shifts)	Definite, assuming $^2\Delta(5d) < {}^2\Pi(5d) < {}^2\Sigma^+(5d)$
$^2\Pi(4d)$	37 984.73(15)	81.49(8)	1.46(1)	1139.4	0.501	0.574	0.073	$\Delta v' = +1$ possible but unlikely	Definite, assuming $^2\Delta(4d) < {}^2\Pi(4d) < {}^2\Sigma^+(4d)$
$^2\Sigma^+(6d)$	43 350.43(9)	80.05(13)	1.63(3)	1010.8	0.478	0.834	0.356	Tenuous at best	Could be $^2\Sigma^+(7s)$ or a mixed $^2\Sigma^+(7s$–$6d)$ state
$^2\Sigma^+(5d)$	41 521.99(35)	73.17(27)	1.55(3)	906.4	0.503	0.739	0.236	Definite (isotope shifts)	Definite, assuming $^2\Delta(5d) < {}^2\Pi(5d) < {}^2\Sigma^+(5d)$
$^2\Sigma^+(4d)$	38 657.85	43.88	0.95	466.3	0.362	0.574	0.212	Definite (Strong origin band)	Definite, assuming $^2\Delta(4d) < {}^2\Pi(4d) < {}^2\Sigma^+(4d)$
$^2\Delta(4f)$	40 113.43(124)	91.12(60)	1.55(5)	1400.0	−0.008	0.029	0.037	$\Delta v' = \pm 1$ likely; ± 2 possible	Definitely $4f$, probably $^2\Delta$
$^2\Pi(4f)$	40 186.73(200)	91.57(108)	1.85(11)	1326.7	−0.030	0.029	0.059	$\Delta v' = \pm 1$ likely; ± 2 possible	Definitely $4f$, probably $^2\Pi$
$^1\Sigma^+$(ion)	46 944.7(20)			1528.5(20)					

[a] Throughout this table, 1σ error estimates are quoted in units of the least significant reported digit, in parentheses following each entry.

[b] Rotational constants for $H\,^2\Sigma^+(5s)\ ^{27}Al\,^{84}Kr$ from Ref. 16: $B_e = 0.085\,97(58)$; $\alpha_e = 0.001\,36(19)$; $\gamma_e = -0.000\,065(10)$; $r_e = 3.10(1)$ Å.

[c] Rotational constants for $B\,^2\Sigma^+(4s)\ ^{27}Al\,^{84}Kr$ from Ref. 16: $B_e = 0.090\,15(39)$; $\alpha_e = 0.001\,24(11)$; $\gamma_e = -0.000\,091(10)$; $r_e = 3.03(1)$ Å.

[d] Rotational constants for $X_1\,^2\Pi_{1/2}(3p)\ ^{27}Al\,^{84}Kr$ from Ref. 16: $B_e = 0.0559(5)$; $\alpha_e = 0.0023(5)$; $r_e = 3.84(1)$ Å.

[e] From Ref. 13.

and $^2\Pi(np)$ series as well, at least over the limited range of n which has been investigated. The $^2\Sigma^+(ns)$ states, on the other hand, show an erratic, nonmonotonic dependence of ω_e on n in both the AlAr and AlKr complexes. This is very likely tied to the fact that a $^2\Sigma^+$ state derives from every separated atom limit in the range from the ground state up to the ionization limit, with the sole exception of the $3s^13p^2,^4P$ state of the aluminum atom. As a result, there are far more opportunities for avoided curve crossings among the $^2\Sigma^+$ states than among any other symmetry species. Such avoided curve crossings can distort the shape of the potential-energy curves substantially, thereby affecting the vibrational frequency. Of course, avoided crossings can also lead to predissociation through nonadiabatic coupling effects, as is also observed in these complexes.

It is interesting to note that the $^2\Delta(nd)$ and $^2\Pi(nd)$ series of AlAr show a convergence of ω_e to a value of approximately 84 cm^{-1}. The less-extensive data which are available for AlKr show the $^2\Delta(nd)$ series converge to a value of $\omega_e \approx 96$ cm^{-1}. Based on these results, the vibrational frequencies of the $AlAr^+$ and $AlKr^+$ ions probably fall in the range of 89 ± 6 and 100 ± 6 cm^{-1}, respectively.

B. The effect of the rare-gas ligand on the Rydberg electron

In addition to considering how the excitation of the $3p$ electron affects the bonding between the rare gas and the aluminum, the data of Tables I and II may be used to consider how the presence of a rare-gas ligand affects the Rydberg electron. This is most naturally accomplished by considering the quantum defect Δ associated with a given Rydberg state. The quantum defect Δ may be calculated from the T_0 values given in the tables by the empirical formula

$$T_0 = \mathrm{IP} - R/(n-\Delta)^2, \tag{4.1}$$

where IP is the adiabatic ionization potential of the complex, R is the Rydberg constant (109 737.318 cm^{-1}),[30] and n is the principal quantum number. For convenience, the quantum defects of the various observed states are listed in Tables I and II, along with the corresponding quantum defects calculated for the isolated aluminum atom. In addition, the difference $\Delta(\mathrm{Al}) - \Delta(\mathrm{complex})$ is tabulated as well, to emphasize the effect of the rare gas on the Rydberg electron.

In addition to the purely empirical Rydberg formula (4.1), the quantum defect Δ may be understood as the phase shift in the radial portion of the wave function of the Rydberg electron, relative to the corresponding radial wave function of a hydrogenic atom.[30,35] Thus, a positive quantum defect (as is commonly the case) corresponds to a contraction of the Rydberg orbital relative to the corresponding hydrogenic orbital. The large quantum defects found for ns orbitals (1.75–1.82 for aluminum, $n = 4$–10) arise because these orbitals penetrate quite effectively, allowing the Rydberg electron to feel a greater positive charge in the region near the nucleus. This causes the ns orbital to contract substantially relative to the hydrogenic case, giving rise to a large phase shift which is reflected in the large quantum defect. Less-penetrating orbitals exhibit smaller quantum defects, in the range of 1.25–1.5 for the np orbitals ($n = 3$–7), 0.36–0.95 for the nd orbitals ($n = 4$–11), and 0.029–0.036 for the nf orbitals ($n = 4$–7).

In all cases we find that the quantum defect for the aluminum rare-gas complex is smaller than that of the isolated aluminum atom. This indicates that the Rydberg orbital of the complex is *expanded* relative to that of the isolated aluminum atom. This result is intuitively satisfying, since the rare gas may be considered as an impenetrable object which excludes a certain volume of space from the Rydberg electron. To compensate for this excluded volume, the Rydberg orbital expands slightly, thereby reducing the quantum defect. This picture is further borne out by the fact that the reduction in the quantum defect which accompanies the formation of the complex is quite small for the $^2\Delta(nd)$ states. In these states the Rydberg electron is located far off the axis of the complex, so the presence or absence of a rare-gas ligand in the axial position is rather immaterial. In contrast, the $^2\Pi(nd)$ states show a significantly greater reduction in quantum defect in going from the atom to the complex, since the rare gas is now interfering with the motion of the Rydberg electron. This interference reaches a culmination in the $^2\Sigma^+(nd)$ states, where the Rydberg orbital is localized along the internuclear axis. In these cases the quantum defect is severely reduced from the free-atom value, indicating that the ligand interferes strongly with the motion of the Rydberg electron.

In support of the idea that the ligand affects the quantum defect by excluding a certain volume of space from the Rydberg electron, we find that the quantum defects associated with the AlKr complex are more greatly reduced from the atomic values than are the quantum defects associated with AlAr, particularly for the strongly interfering $^2\Sigma^+(nd)$ states. Indeed, it is only in the weakly interfering $^2\Delta(nd)$ states and a few of the $^2\Sigma^+(ns)$ states that the reverse situation is encountered. This is consistent with the idea that a krypton atom excludes more space from the Rydberg electron than does the smaller argon atom.

By excluding a volume of space which would ordinarily be available for the motion of the Rydberg electron, the rare gas can actually reverse the sign of the quantum defect, resulting in a net expansion of the Rydberg orbital beyond the size expected for a hydrogenic system. This is evident in the quantum defects associated with the $4f$ and $5f$ Rydberg states in both AlAr and AlKr [with the exception of the $^2\Delta(4f)$ and $^2\Delta(5f)$ states of AlAr]. In these cases the atomic quantum defect is quite small, because of the nonpenetrating nature of the f orbitals. Accordingly, the radial portion of the f orbitals of aluminum is very similar to hydrogenic f orbital radial functions. In this case, the net expansion of the f-based Rydberg orbital due to the excluded volume occupied by the rare gas actually causes the orbital to become larger in the complex than in the hydrogen atom. In the terminology of scattering theory (which can be used as a basis for quantum defect theory),[35] the scattering of the Rydberg electron by repulsive interactions with the electrons of the rare gas dominates (in the case of an f-Rydberg electron) over the scattering due to attractive interactions with the aluminum core, leading to a net negative phase shift

(or a negative quantum defect). In all other observed states listed in Tables I and II (which all possess $l<3$), attractive interactions with the aluminum core dominate over the repulsive interactions with the rare-gas atom, leading to a net positive phase shift in the Rydberg orbital wave function, giving a positive quantum defect.

V. SUMMARY

The spectra of the van der Waals complexes AlAr and AlKr have been examined using the technique of resonant two-photon ionization spectroscopy in a skimmed, jet-cooled molecular beam, with mass spectrometric detection. In both complexes spectra have been obtained from 31 000 cm^{-1} to the ionization limit. The adiabatic ionization potentials of both molecules have been determined by measuring the threshold for one-photon ionization and correcting for the field-ionization shift, giving IP(AlAr) $= 47\,418.5 \pm 2$ cm^{-1} $(5.8791 \pm 0.0002$ eV) and IP(AlKr) $= 46\,944.7 \pm 2$ cm^{-1} $(5.8204 \pm 0.002$ eV). In both cases a much weaker preliminary threshold has been observed some 80 cm^{-1} to the red, which is interpreted as the ionization threshold of a small population of spin–orbit excited, $X_2\,^2\Pi_{3/2}(3p)$ states in the jet-cooled molecular beam. This assignment allows the spin–orbit splitting of the $X\,^2\Pi(3p)$ state to be estimated as 80.9 ± 2 cm^{-1} and 78.4 ± 4 cm^{-1} for AlAr and AlKr, respectively. Although the thresholds are not as abrupt as in the cases of AlAr and AlKr, adiabatic ionization potentials of $AlAr_2$ and $AlAr_3$ have been estimated as $46\,660.3 \pm 2$ cm^{-1} $(5.7851 \pm 0.0002$ eV) and 46 295 cm^{-1} (5.7399 eV), respectively.

Vibronic spectra of the fully allowed $3s^2ns^1,^2S_{1/2} \leftarrow 3s^23p^1,^2P^0$ and $3s^2nd\,^1,^2D_{1/2} \leftarrow 3s^23p^1,^2P^0$ transitions in the aluminum atom have been observed in the AlAr and AlKr complexes, where they have been designated as the $^2\Sigma^+(ns) \leftarrow X_1\,^2\Pi_{1/2}(3p)$, $^2\Delta(nd) \leftarrow X_1\,^2\Pi_{1/2}(3p)$, $^2\Pi(nd) \leftarrow X_1\,^2\Pi_{1/2}(3p)$, and $^2\Sigma^+(nd) \leftarrow X_1\,^2\Pi_{1/2}(3p)$ systems. Isotope shifts between the $^{27}Al\,^{82}Kr$ and $^{27}Al\,^{86}Kr$ isotopic modifications have been used to secure the vibrational numbering in the krypton complex, and the rule that the bond strength should uniformly increase with increasing n in a given Rydberg series has been used to aid in the vibrational numbering in the AlAr spectra.

The spectra of the $3d \leftarrow 3p$ transition are quite complicated in both species, probably because of strong mixing between the 3*d*- and 4*p*-based states. Nevertheless, an important piece of information is obtained by an analysis of the spectra of this region (31 500–32 700 cm^{-1}). High vibrational levels of the 3*d*-based states [probably of the $^2\Sigma^+(3d)$ state] are observed in both molecules all the way to the convergence limit. This allows the bond strengths to be determined as $D_0[\text{AlAr}, X_1\,^2\Pi_{1/2}(3p)] = 122.4 \pm 4$ cm^{-1} and $D_0(^{27}Al\,^{84}Kr) = 194.7 \pm 0.8$ cm^{-1}. These values may then be combined with the measured ionization potentials to derive bond strengths of the cations as $D_0(Al^+\text{–Ar}) = 982.3 \pm 5$ cm^{-1} and $D_0(Al^+\text{–Kr}) = 1528.5 \pm 2$ cm^{-1}.

In addition to following the spectra of the fully allowed $ns \leftarrow 3p$ and $nd \leftarrow 3p$ systems out to high values of n, we have observed several transitions that are forbidden in the aluminum atom, which become weakly allowed in the complexes. These include the $4f \leftarrow 3p$, $5f \leftarrow 3p$, and $6p \leftarrow 3p$ transitions, which are forbidden in the atom under electric dipole selection rules. Their occurrence in the complex, however weakly, is a direct result of the reduction in symmetry which accompanies complex formation, and indicates a distortion of the aluminum orbitals away from their shape in the isolated atom. A measurement of the absolute intensity of these systems would provide a very interesting measure of the degree of distortion experienced by the atomic orbitals when the complex is formed.

We also note that certain band systems appear at the mass of the aluminum atom, and this is interpreted as resulting from a rapid predissociation of the excited Rydberg state, forming an aluminum atom in an *excited* electronic state. This excited electronic state is then readily ionized by absorption of a second photon, resulting in the observation of a spectrum of the complex at the mass of the atom. Indeed, some band systems are only observed at the atomic mass, indicating facile predissociation dynamics, while others are observed only at the mass of the complex. In other cases the fragmentation quantum yield varies dramatically with vibrational level and with electronic state in a given energy range, indicating that a rich dynamical process is occurring. Since so many of the excited electronic states of these complexes are spectroscopically accessible, an unusually complete picture of dissociation dynamics in the presence of many potential-energy surfaces could be gained by further investigations.

Finally, we note that the properties of the $^2\Delta(nd)$ and $^2\Pi(nd)$ states appear to converge smoothly toward the properties of the cation, allowing the cationic vibrational frequencies to be estimated as 89 ± 6 and 100 ± 6 cm^{-1}, for $AlAr^+$ and $AlKr^+$, respectively. Likewise, the effect of the rare-gas atom on the Rydberg electron has been examined by a study of the quantum defects of the various Rydberg series. In all cases, the presence of the rare-gas serves to decrease the quantum defect in the complex from that of the free aluminum atom, particularly in cases where the Rydberg electron is localized to some degree on the internuclear axis [as in $^2\Sigma^+(nd)$ states]. This indicates that the wave function of the Rydberg electron is expanded in the complex as compared to the free atom. This is interpreted as resulting from the exclusion of a certain volume to the Rydberg electron, which forces the Rydberg orbital to expand. Alternatively, in the language of scattering theory, the repulsive interactions between the Rydberg electron and the electrons of the rare-gas atom cause the scattering phase shift to be more negative than would otherwise be the case, thereby counteracting to some degree the attractive interactions with the aluminum atom core. This reduces the quantum defect, allowing the Rydberg orbital to expand and be less tightly bound than would otherwise be expected.

ACKNOWLEDGMENTS

We thank Professor William H. Breckenridge for the use of the intracavity étalon employed in the high-resolution

studies. We gratefully acknowledge research support from NSF under Grant No. CHE-8912673. Acknowledgment is also made to the donors of the Petroleum Research Fund, administered by the American Chemical Society, for partial support of this research.

[1] R. E. Smalley, B. L. Ramakrishna, D. H. Levy, and L. Wharton, J. Chem. Phys. **61**, 4363 (1974).
[2] R. E. Smalley, L. Wharton, and D. H. Levy, J. Chem. Phys. **63**, 4977 (1975).
[3] R. E. Smalley, D. A. Auerbach, P. S. H. Fitch, D.H. Levy, and L. Wharton, J. Chem. Phys. **66**, 3778 (1977).
[4] J. Tellinghuisen, A. Ragone, M. S. Kim, D. J. Auerbach, R. E. Smalley, L. Wharton, and D. H. Levy, J. Chem. Phys. **71**, 1283 (1979).
[5] C. Dedonder-Lardeux, C. Jouvet, M. Richard-Viard, and D. Solgadi, J. Chem. Phys. **92**, 2828 (1990).
[6] C. Jouvet, C. Lardeux-Dedonder, S. Martrenchard, and D. Solgadi, J. Chem. Phys. **94**, 1759 (1991),
[7] P. Y. Cheng, K. F. Willey, and M. A. Duncan, Chem. Phys. Lett. **163**, 469 (1989).
[8] R. E. Smalley, D. H. Levy, and L. Wharton, J. Chem. Phys. **64**, 3266 (1976).
[9] R. E. Smalley, L. Wharton, and D. H. Levy, J. Chem. Phys. **68**, 671 (1978).
[10] D. Frye, P. Arias, and H.-L. Dai, J. Chem. Phys. **88**, 7240 (1988).
[11] C. L. Morter, A. Koskelo, Y. R. Wu, and D. H. Levy, J. Chem. Phys. **89**, 1867 (1988).
[12] J. M. Gardner and M. I. Lester, Chem. Phys. Lett. **137**, 301 (1987).
[13] C. L. Callender, S. A. Mitchell, and P. A. Hackett, J. Chem. Phys. **90**, 5252 (1989).
[14] C. L. Callender, S. A. Mitchell, and P. A. Hackett, J. Chem. Phys. **90**, 2535 (1989).
[15] M. J. McQuaid, J. L. Gole, and M. C. Heaven, J. Chem. Phys. **92**, 2733 (1990).
[16] Z.-W. Fu, S. Massick, J. G. Kaup, O. B. d'Azy, and W. H. Breckenridge, J. Chem. Phys. **97**, 1683 (1992), preceding paper.
[17] K. E. Schriver, M. Y. Hahn, J. L. Persson, M. E. La Villa, and R. L. Whetten, J. Phys. Chem. **93**, 2869 (1989).
[18] Z.-W. Fu, G. W. Lemire, G. A. Bishea, and M. D. Morse, J. Chem. Phys. **93**, 8420 (1990).
[19] E. S. Chang, J. Phys. Chem. Ref. Data **19**, 119 (1990).
[20] Z.-W. Fu, G. W. Lemire, Y. Hamrick, S. Taylor, J.-C. Shui, and M. D. Morse, J. Chem. Phys. **88**, 3524 (1988).
[21] S. C. O'Brien, Y. Liu, Q. Zhang, J. R. Heath, F. K. Tittel, R. F. Curl, and R. E. Smalley, J. Chem. Phys. **84**, 4074 (1986).
[22] C. E. Moore, Natl. Bur. Stand. Circ. 467 (U.S. GPO, Washington, DC, 1949, 1952).
[23] S. Gerstenkorn and P. Luc, *Atlas du Spectre d'Absorption de la Molecule d'Iode* (CNRS, Paris, 1978); S. Gerstenkorn and P. Luc, Rev. Phys. Appl. **14**, 791 (1979).
[24] G. A. Bishea, N. Marak, and M. D. Morse, J. Chem. Phys. **95**, 5618 (1991).
[25] G. A. Bishea, J. C. Pinegar, and M. D. Morse, J. Chem. Phys. **95**, 5630 (1991).
[26] S. Taylor, E. M. Spain and M. D. Morse, J. Chem. Phys. **92**, 2698 (1990).
[27] J. L. Persson and R. L. Whetten, Chem. Phys. Lett. **147**, 168 (1988).
[28] V. S. Letokhov, *Laser Photoionization Spectroscopy* (Academic, Orlando, FL, 1987), pp. 71–79.
[29] D. S. Bailey, J. R. Hiskes, and A. C. Riviere, Nucl. Fusion **5**, 41 (1965).
[30] H. Lefebvre-Brion and R. W. Field, *Perturbations in the Spectra of Diatomic Molecules* (Academic, Orlando, FL, 1986), pp. 90, 91, 214, and 216–220.
[31] See AIP document No. PAPS JCPSA-97-1692-16 for 16 pages of tables of band positions. Order by PAPS number and journal reference from American Institute of Physics, Physics Auxiliary Publication Service, 335 East 45th Street, New York, NY 10017. The price is $1.50 for each microfiche (60 pages) or $5.00 for photocopies of up to 30 pages, and $0.15 for each additional page over 30 pages. Airmail additional. Make checks payable to the American Institute of Physics.
[32] M. Hliwa and J.-P. Daudey, Chem. Phys. Lett. **153**, 471 (1988).
[33] M.-C. Duval, O. B. D'Azy, W. H. Breckenridge, C. Jouvet, and B. Soep, J. Chem. Phys. **85**, 6324 (1986).
[34] W. L. Wiese, M. W. Smith, and B. M. Miles, *Atomic Transition Probabilities*, Natl. Stand. Ref. Data Ser. Natl. Bur. Stand 22 (U.S. GPO, Washington, DC, 1969), pp. 48–49.
[35] C. H. Greene and Ch. Jungen, Adv. Atom. Mol. Phys. **21**, 51 (1985).